Presented at the Seattle, Washington
Electrochemical Society Conference,
Seattle, WA, May 22 - 26, 1978

LBL-7331
C. 2

ELEVATED TEMPERATURE CORROSION BEHAVIOR OF IRON-BASE TERNARY ALLOYS THAT DEVELOP Cr_2O_3 AND/OR Al_2O_3 BARRIER SCALES

V. Nagarajan and A. V. Levy

May 1978

Prepared for the U. S. Department of Energy
under Contract W-7405-ENG-48

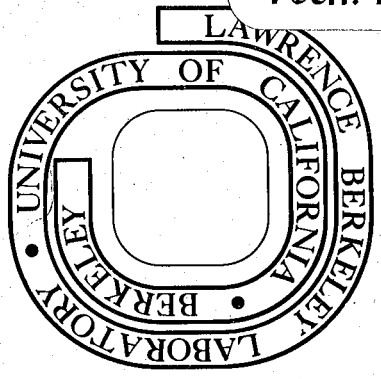

LBL-7331
C. 2

ELEVATED TEMPERATURE CORROSION BEHAVIOR OF IRON-BASE TERNARY ALLOYS THAT DEVELOP Cr_2O_3 AND/OR Al_2O_3 BARRIER SCALES*

V. Nagarajan and A.V. Levy

Materials and Molecular Research Division
Lawrence Berkeley Laboratory

ABSTRACT

The elevated temperature corrosion behavior of iron-base ternary alloys that develop Cr_2O_3 and/or Al_2O_3 barrier scales was investigated by exposing them to a mixed gas environment at 982°C whose P_{O_2} was approximately 10^{-18} atm and whose P_{S_2} was approximately 10^{-6} atm. The alloys containing 18% Cr and 2.5-5% Al had the best corrosion resistance of the alloys tested. They developed a duplex Cr_2O_3/Al_2O_3 scale through which sulfur did not readily diffuse. The 18% Cr alloy containing only 1% Al formed a Cr_2O_3 scale and had poor corrosion resistance because of rapid sulfur diffusion through the scale.

Alloys that contained 10% Al and 0-15% Cr did not have good corrosion resistance because of sulfur diffusion through the single Al_2O_3 scale which formed. Alloys with 18% Cr that contained Si as a ternary addition did not develop continuous SiO_2 layers beneath the Cr_2O_3 outer scale and exhibited poor corrosion resistance.

*This work was supported by the Division of Physical Research of the Department of Energy.

INTRODUCTION

The dwindling supply of domestic oil and natural gas has necessitated the development of "coal gasification" processes. Quite a large number of processes are currently being developed and their operating conditions vary over a wide range of temperatures and pressures. A typical coal gasification atmosphere is presented in Table 1 [1] which lists the compositions of the raw gas, the gas equilibrated at 1 atm and 68 atm at 982°C. Analysis of the gas composition indicates that oxygen, sulfur and carbon are the three important corroding species and the ranges of activities of oxygen, sulfur, and carbon are 10^{-16} to 10^{-15} atm, 10^{-6} atm, and 10^{-3} to 10^{-1} atm respectively.

The current generation of commercially available stainless steels and nickel and cobalt base superalloys rely on the selective oxidation of chromium or aluminum or both to form a barrier layer which provides corrosion protection. These alloys were developed primarily for highly oxidizing conditions that exist in power plants and gas turbines. Although large amounts of data are available in the literature [2] on the breakdown mechanism of protective oxide scales in gas turbine environments, very little information is available on the barrier behavior of scales in coal gasification atmospheres. A research program was undertaken to investigate the barrier behavior of scales in coal gasification atmospheres which are not only sulfidizing but also reducing. The investigation has been restricted to iron base alloys that form Cr_2O_3, Cr_2O_3/SiO_2, Cr_2O_3/Al_2O_3, or Al_2O_3 scales. Nickel base and cobalt base alloys have not been included because their sulfides melt much below 982°C. Also, because the formation of a liquid

corrosion product leads to almost immediate catastrophic rates of corrosion, it was decided that iron base alloys may be better than nickel base and cobalt base alloys. Furthermore, availability and economic considerations favor iron base alloys.

The nominal and the actual composition of the alloys investigated are presented in Table 2. The first four alloys containing varying amounts of Si are mainly Cr_2O_3 formers, with Si concentrated at the scale/alloy interface as internal oxide particles. Alloy 5 is also a Cr_2O_3 former with internal Al_2O_3 precipitates. Alloys 6 to 12 are all external Al_2O_3 formers and they contain varying combinations of Cr and Al.

It appears that of the three reactive species in the gas, namely oxygen, sulfur, and carbon, which are of interest from the viewpoint of corrosion, only oxygen and sulfur seem to play major roles [3]. Therefore, this program is mainly aimed at elucidating the barrier behavior of oxide scales to sulfur and oxygen penetration and not carbon penetration.

Thermodynamics demands that any metallic material exposed to an environment containing oxygen and sulfur should form various oxide phases and sulfide phases and that their relative stabilities are controlled not only by their free-energies of formation but also by the PS_2/PO_2 ratio. Information on the relative stabilities of the phases is normally obtained from "phase stability" diagrams. Hemmings and Perkins [4] and Gulbranson and Jansson [5] have developed phase stability relationships for Al, Cr, and Fe in the presence of O and S. With a PO_2 of approximately 10^{-16} atm and PS_2 of approximately 10^{-6} atm

at 982°C (typical of a coal gasifier), according to their diagrams, the stable phases which should form on the surfaces of the alloys investigated are FeS, Al_2O_3, Cr_2O_3, and SiO_2. These authors have neglected the possibility of oxide and sulfide spinel formation which could change the stability of the phases. Recently Gordon et al. [6] have considered the formation of $FeCr_2O_4$ and $FeAl_2O_4$ spinels in plotting their stability diagrams. According to their diagrams, with a PO_2 of 10^{-16} atm and PS_2 of 10^{-6} atm at 982°C, FeS should be unstable. The spinels persist up to an approximate PO_2 of 10^{-17} atm. With a $PO_2 \sim 10^{-18}$ atm and $PS_2 \sim 10^{-6}$ atm, FeS should be stable. Therefore in this investigation a gas mixture was chosen such that the PO_2 was approximately 10^{-18} atm and PS_2 was approximatey 10^{-6} atm, so that the formation of spinels could be excluded and the barrier behavior of the simple oxides could be investigated.

Although the stability diagrams predict that only FeS, Cr_2O_3, Al_2O_3, and SiO_2 will be stable on the surface, compounds such as CrS_x and Al_2S_3 can form within or beneath the surface scales due to the internal variation in PO_2 and PS_2. The formation of these other phases is controlled by the nature of transport of the gaseous as well as metallic species through the outer scales. The complex reactions that may occur have been reviewed by Birks [7] and Rapp [8]. The formation of these phases could be either beneficial or deleterious depending on the nature of the phases and their location. For example, formation of continuous SiO_2 layers beneath Cr_2O_3 surface scales is considered quite beneficial while formation of internal sulfides is deleterious.

In complex gas mixtures, not only atomic species of oxygen and

sulfur can be transported through the scales but also molecular species such as H_2O and H_2S may be transported. At 982°C, grain boundary transport should predominate over bulk diffusion, although there may be some bulk diffusion in Cr_2O_3 scales. No attempt has been made to establish whether molecular species are transported through the scales and their paths of transport.

EXPERIMENTAL

All the alloys were melted in an induction furnace under argon and were cast into 5-lb ingots. The ingots were homogenized at 1200°C for 24 hours and rolled into thin sheets. Sections were then cut from the rolled sheet, annealed, surface ground, and coupons of 1.5 x 1.5 x 0.1 cm were prepared. Holes were drilled for suspending the coupons. The coupons were then ground through 600 grit silicon carbide papers, cleaned with water and degreased with alcohol.

A vertical furnace was used to carry out the corrosion experiments. The furnace consisted of a 2.5 in. i.d. by 24-in. long mullite tube, which was heated to 982°C. The temperature of the furnace was controlled within $\pm$2°C. The specimens were introduced from the top of the furnace using a ceramic specimen-supporting arrangement that extended the specimens in the top half of the furnace tube. The specimens were suspended by Kanthol support wires. The gas mixture consisted of argon, H_2, H_2O, and H_2S. A water bubbler, whose temperature was controlled to within $\pm$0.1°C, was used to pick up H_2O in the gas stream, and argon was used as a carrier gas for picking up H_2O vapor. A prebubbler was also used to ensure complete saturation. The gas flows were

controlled accurately using rotometers. The gas composition was such that the PO_2 was 10^{-18} atm and PS_2 was 10^{-6} atm at 982°C. The gas mixture was introduced at the bottom of the furnace and was allowed to leave from the top. The bottom of the furnace was filled with high purity alumina beads up to the constant temperature zone to ensure thorough mixing and heating of the gas flowing in at a rate of 500-cc/min, so that thermal segregation could be prevented. To prevent condensation of water, the gas inlet and outlet tubes were maintained over 200°C.

After introducing the specimens into the furnace, the system was flushed with argon for 30 min, after which the test gas mixture was admitted into the system. At the end of the run, the system was once again flushed with argon for 30 min. Then, the specimens were quickly removed from the furnace and allowed to cool rapidly.

The corroded specimens were carefully removed and weighed. The specimen surfaces and cross sections were examined using optical and scanning electron microscopes. Phase analyses were carried out using EDAX and x-ray diffraction. The cross sections were prepared by mounting the specimens in bakelite and grinding through 600-grit silicon carbide papers and finer diamond and alumina polishing wheels.

Specimens were also corroded after preoxidizing for three days at 982°C in an air atmosphere. This treatment is referred to as "preoxidation" in the text.

RESULTS

The weight gain/unit area data for all the 12 alloys corroded without preoxidation are presented in Table 3 and also graphically in Figures 1(abc) through 1(ikl). Due to the nature of the apparatus used, continuous monitoring of the weight gain data was not possible. The data were obtained over duplicate runs. Figures 1(abc) and 1(d) describe the weight gain/unit area versus time plots for the silicon containing alloys 1 to 4. All the alloys except alloy 4 show large weight gain right from the beginning, and continuing corrosion. Most of the specimens were almost totally corroded after about three days. Alloy 4 shows good corrosion resistance up to about two days but after that it corrodes fairly rapidly. The weight gain/unit area after five days is only about 10% of that of the other three alloys.

Figures 1(e) to 1(gh) describe the weight gain/unit area versus time plots for the 18% Cr alloys numbered 5 to 8. Alloy 5 is fairly resistant up to 24 hr, but corrodes catastrophically after that. Alloy 6 shows good corrosion resistance up to five days. Although the curve appears to be parabolic, its true nature is not known due to the method used for collecting the data. Some points show negative weight gain and they were due to scale spallation. Figure 1(gh) is similar to Figure 1(f) and the alloys seem to show poor corrosion resistance with increasing Al content. Although the weight gain/unit area for alloy 8 after five days is only 2-1/2 times that for alloy 6, the specimen has suffered severe local corrosion. Figure 1(ikl) shows the plots of weight gain/unit area versus time for the 10% Al alloys 9 to 12. All the alloys have suffered severe corrosion and the weight gain data after five days shows a ten to twentyfold increase in comparison to alloys 6 to 8, except for alloy 10. Although alloy 10 does not show

large weight gain after five days, a single specimen of the alloy shows a large weight gain (and severe corrosion) after 24 hours [Figure (1-j)]. It is not conclusive whether the alloy has good or poor corrosion resistance, but since a couple of specimens were badly corroded, it has been assumed that this alloy also has poor corrosion resistance.

Preoxidation treatment improved the corrosion resistance of all the alloys; the greatest improvement occurred in alloys which had the poorest corrosion resistance in the initial tests.

Figures 2 to 4(b) show the external appearances of the alloys which had poor corrosion resistance. In Figure 2, the progression of corrosion on alloy 2 with time is shown; the corrosion has started near the holes and edges and has spread to the rest of the area. Figure 3 shows the influence of increasing the Si content after two and five days of corrosion. Again, the corrosion has started near the edges and corners. Figures 4(a) and 4(b) show the effect of the preoxidation treatment on corrosion after two days for the alloys containing Si and the alloys containing 10% Al. It is evident that preoxidation has resulted in an improved corrosion resistance.

CORROSION MORPHOLOGIES

The twelve alloys were separated into two groups based on the type of external scales developed. The first group consisted of alloys 1 through 5 which developed external Cr_2O_3 scales. Alloys 6-12 developed external Al_2O_3 scales and they made up the second group.

External Cr_2O_3 Formers

The Si-containing alloys initially developed thin Cr_2O_3 scales.

Sulfur penetrated through the scale and formed sulfides beneath the oxide scale, causing scale breakaway. For example, Figure 5 shows the formation of sulfides beneath oxide, causing the oxide to crack. Figure 5(a) shows the secondary electron image of a specimen of alloy 2 corroded for one day, at a magnification of 200X. Figure 5(bcd) shows the S, Fe, and Cr x-ray maps. The area marked "A" on Figure 5(a) shows enrichment in chromium with no S or Fe, and so it is chromium oxide. Also, the S-enriched area shows the presence of Fe and Cr and it is highly probable that it is a complex Fe-Cr sulfide.

Figure 6 shows the cross section of the scale formed on alloy 1 corroded for one day at a magnification of 128X. The specimen has developed a thick and columnar, outer Fe-rich, Fe-Cr complex sulfide. The inner scale marked "B" consists of a mixture of Cr_2O_3 and the complex sulfide. There are a few internal precipitates of SiO_2 and complex Fe-Cr sulfides in the alloy matrix. On further exposure, the inner scale layer has thickened. Figure 7 shows the specimen of alloy 1 corroded for two days at a magnification of 160X. The outer layer has spalled off. The alloy has developed extensive amounts of internal sulfides.

Similar behavior is also observed with the higher Si-containing alloys. Figure 8 shows the scale morphology of a specimen of Fe-18Cr-2Si and it is very similar to the scale morphology shown in Figure 6. Figure 9 shows the secondary electron image and the x-ray maps of the same specimen shown in Figure 8 and the area near outer scale/inner scale interface is only analyzed (at a magnification of 250X). The unreacted pure Fe regions are clearly visible. Again,

the sulfides appear to contain both Fe and Cr as is seen in the EDAX image. Furthermore, comparing the Cr and S x-ray maps, it is seen that there are regions which contain only Cr (and no S and Fe) and these are chromium oxides. (The oxide phase is indicated in the secondary electron image.)

After preoxidation and subsequent corrosion, similar morphologies are observed although the onset of rapid corrosion is delayed.

Although alloy 5 contains about 1% Al, it has not developed an external Al_2O_3 scale. Instead, it has developed an external Cr_2O_3 scale with a few precipitates of internal Al_2O_3 particles. Like the Si-containing alloys which form Cr_2O_3 scales, alloy 5 also has suffered extensive corrosion. Figure 10a shows the scale morphology of a specimen corroded for three days and Figure 10b shows the scale/alloy interface. The outer scale consists of columnar Fe-Cr sulfide. The internal precipitates are mainly Cr sulfides as shown in Figure 11. Preoxidation has again slowed down the rate of corrosion.

External Al_2O_3 Formers

There are two series of alloys which form Al_2O_3 scales--the ones containing approximately 18% Cr and 3%, 5%, and 7% Al and the ones containing approximately 10% Al and 0%, 5%, and 15% Cr.

Alloys 6 and 7 suffered little corrosion up to five days. They developed thin protective external Al_2O_3 scales with little internal penetration. Although alloy 8 developed external Al_2O_3 scale, it corroded. Figure 12 shows the secondary electron image and the x-ray maps of a specimen of alloy 8 corroded for 5 days at a magnification

of 150X. The outer portion of the scale consists of Cr-rich complex sulfide. The inner scale consists of a porous and thick Al_2O_3 layer. The presence of internal Al_2O_3 and CrS_x are also noted. Figure 13 shows the scale/alloy interface at a higher magnification. The x-ray maps reveal the presence of Al_2O_3, Cr_2O_3, and CrS_x phases. Preoxidation has improved the corrosion resistance considerably. All the preoxidized specimens have developed thin Al_2O_3 scales with no internal corrosion.

All the alloys containing 10% Al have corroded extensively. Figure 14 shows a specimen of alloy 9 corroded for two days. It has developed extensive amounts of outer FeS ($+Al_2O_3$) layers and extensive amounts of internal Al_2O_3 particles (Figure 15). The corrosion morphologies of alloys 10-12 are similar to those of alloy 9, except for the appearance of Cr-rich sulfides in the alloy matrix. Figure 16 shows the cross section of a specimen of alloy 12. The specimen has been completely penetrated by internal CrS_x. Prolonged exposures have caused more corrosion and the appearance of Fe-Cr-S external layers.

Preoxidation considerably improved the corrosion resistance of all the alloys. All the alloys developed thin Al_2O_3 scales with no internal penetration.

DISCUSSION

According to the phase stability diagrams of Gordon et al. [6], at a PO_2 of 10^{-18} atm and PS_2 of 10^{-6} atm, the stable phases on the surface should be oxides of Cr, Al, and FeS. The solubility of Cr in FeS has been discounted due to the lack of sufficient data. Although

the phase stability diagrams indicate that the sulfide is FeS, the experimental observation suggests that the sulfide is indeed a complex Fe-Cr sulfide.

The discussion has been divided into two portions. The first portion deals with alloys that form Cr_2O_3 scales and the second portion deals with alloys that form Al_2O_3 scales.

Cr_2O_3 Formers

A series of commercial stainless steels that have been developed in the past with about 18% Cr form external Cr_2O_3 scales. It is not surprising that alloys 1 through 5, which contain about 18% Cr, are also external Cr_2O_3 scale formers. The alloys containing Si showed the presence of internal oxides of SiO_2, but even with 2% Si, continuous layers of SiO_2 do not seem to be forming and covering the entire scale/alloy interface. Increasing the Si content to 2% does, however, slow down the rate of corrosion. To be more accurate, the onset of rapid corrosion is delayed and this must be due to the establishment of SiO_2 layers, if not across the entire scale/alloy interface, at least at some areas.

The stability of Fe-(Cr)-sulfides on the surfaces of these alloys plays a significant role in their corrosion behavior. Similar alloys, exposed by Perkins et al. [9] to a slightly higher PO_2 gas (approximately 10^{-16} atm) at 982°C, where FeS should be unstable, showed better corrosion resistance.

All these alloys should nucleate FeS (or Fe-Cr-S), Cr_2O_3, and SiO_2 particles as soon as the fresh surfaces are exposed to the corrosive

gas. With increase in the time of exposure, these nuclei should grow. Because the amount of Si is very small, the number of nuclei of SiO_2 will be small. But the number of Cr_2O_3 nuclei will be very large and the number of nuclei of the sulfide should be in between these two. Once the nuclei grow and cover the entire surface, the scale would consist of Cr_2O_3 containing some sulfide particles. If the sulfides are established as channels in Cr_2O_3, connecting the alloy matrix with the corrosive gas, severe corrosion will occur beneath the channels due to rapid diffusion of S and Fe through the sulfide channels. Essentially, the sulfides will be providing short circuit paths. Figure 17 shows a specimen of alloy 3 exposed to corrosive gases for 24 hr. The surface consists of Cr_2O_3 mixed with sulfides, which should be present in the form of channels. Further evidence for the sulfide channels comes from Figure 18(abcd), which shows an area very close to the scale/alloy interface of the alloy containing 1-5 Si. In Figure 18, "A" shows the secondary electron image magnified at 2KX while "B", "C" and "D" show iron, sulfur and chromium maps respectively. The Cr_2O_3 scale near the metal interface is interspersed with sulfide channels. Preoxidation treatment delays the onset of catastrophic corrosion. The preoxidation in air should develop a scale without any sulfide channels, so the corrosion behavior of the alloy is improved. If sulfide channels were not formed from the beginning in specimens not preoxidized there would be no difference between the rates of corrosion without and with preoxidation.

Furthermore, the fact that the preoxidation treatment only delays the onset of rapid corrosion and does not prevent catastrophic corrosion

indicates that elimination of the initially-forming sulfide channels in Cr_2O_3 is not sufficient for corrosion protection, and that Cr_2O_3 must be allowing S to diffuse through. There is a considerable body of evidence in the literature that shows that Cr_2O_3 scales do not prevent S from diffusing inwards.

Al_2O_3 Formers

The Al_2O_3 forming alloys show an interesting corrosive behavior. Conventional analysis would indicate that the alloys rich in Al (or Al+Cr) should show better corrosion resistance than the alloys lean in Al because these alloys can sustain the barrier scale for prolonged periods. One would, therefore, have expected alloys 8, 11, and 12 to be more resistant than alloy 6, but the experimental results indicate the opposite.

The observed behavior could be explained if there was a considerable difference between the morphology and grain size of Al_2O_3 in alloys 8, 11, and 12 and the morphology and grain size of Al_2O_3 in 6. However, the oxidation studies carried out do not reveal enough of a difference in the oxide morphology to account for such a drastic corrosion behavior [10].

The second possibility is that Al_2O_3 may be cracking extensively in alloys 8 to 12 due to growth stresses and not in alloys 6 and 7 which have a lower aluminum content. Observation of the morphologies of the oxides growing on these alloys excludes this possibility. There is very little evidence [10] for cracking due to growth stresses in the Al_2O_3 scale formation. In iron-base alloys, approximately 7% Al is

required to form external Al_2O_3 scales and about 18% Cr to form external Cr_2O_3 scales. A binary Fe-2.5% Al alloy does not form an external Al_2O_3 scale unless about 16% to 18% Cr is added as an oxygen getter. The mechanism of Al_2O_3 scale formation in the low Al, high Cr alloys is a well understood phenomenon [12,13]. Initially, the alloy develops an extremely thin Cr_2O_3 scale which slows down the influx of oxygen (hence the PO_2) to the scale-metal interface, thus allowing sufficient time for Al to oxidize and grow as a continuous layer beneath the Cr_2O_3 layer. Essentially, the alloys develop duplex Cr_2O_3/Al_2O_3 layers, with the Cr_2O_3 layer being very thin.

Increasing the Al content to higher levels would ease the establishment of an Al_2O_3 layer. In other words, at around 7% Al, development of a Cr_2O_3 layer is not a prerequisite for the establishment of an Al_2O_3 layer, and Al_2O_3 can form as a single layer.

The volume of the single Al_2O_3 layer, instead of the duplex Cr_2O_3/Al_2O_3 layer, should increase as the Al content increases. So, only alloys 6 and 7 would be expected to have greater amounts of duplex Cr_2O_3/Al_2O_3 scale while the other alloys would be expected to have a higher proportion of single Al_2O_3 scale.

In the single Al_2O_3 scale, there will be a considerable drop in the PO_2 (the initial value in the gas is 10^{-18} atm) across the scale; thus as Cr diffuses from the bulk to the grain boundaries of Al_2O_3, there is a good chance that it will form a sulfide instead of an oxide. The formation of the sulfide in the Al_2O_3 grain boundaries is seen in Figure 18.

Sulfide formation should lead to cracking of the Al_2O_3 scale due

to the large volume change. Furthermore, the plasticity of the sulfides would cause them to be extruded out to the gas-scale interface along the grain boundaries of Al_2O_3, thereby also causing the scale to crack. The repeated process of cracking would cause the further formation of Al_2O_3, creating a massive layer of Al_2O_3 and leading to a drastic depletion of Al from the alloy. Figure 19 shows the large Al-depleted zone in the alloy matrix. At some stage, the alloy would lose the ability to form an Al_2O_3 scale and hence corrode catastrophically.

The evidence for the formation of duplex Cr_2O_3/Al_2O_3 scale comes from Figure 20 (abcd). The x-ray maps for Cr and S show a region which is rich in Cr, but containing no S. This region is Cr_2O_3 and is present on top of the Al_2O_3 scale. Sulfur has not penetrated this scale while the single scale of Al_2O_3 has been penetrated. Furthermore, the cracking of Al_2O_3 by CrS_x is also evident (as pointed out in the figure). The exact reasons why sulfides are not formed within the duplex scale and why S may not be diffusing through are not known. It could be speculated that the ratio of PO_2 and PS_2 across the duplex scale is such that the formation of CrS_x is unlikely. Further research is required to understand the exact mechanism.

The best corrosion resistance is exhibited by Fe-17Cr-2.5Al alloy and Fe-26Cr-4Al (kanthol support wires) alloy. The ratio of Cr to Al in both the alloys is almost identical and it appears that this ratio may be of some significance.

Similar results were obtained by Perkins et al. [9]. In their experiments, they observed the high Al alloys to have poor corrosion

resistance.

CONCLUSIONS

The alloys that form Cr_2O_3 as the principal barrier scale have extremely poor corrosion resistance. The addition of Si has very little influence on corrosion except at the 2% level, where it delays the onset of rapid corrosion. However, even at the 2% Si level, continuous layers of SiO_2 are not established. In all these alloys, S penetrates the Cr_2O_3 scale through FeS channels in the oxide.

The corrosion resistance of alloys that form Al_2O_3 barrier scales is dependent on the level of Al in the alloys. Alloys that contain small amounts of Al (3 - 5%) show good corrosion resistance while alloys that contain more than 7% Al show poor corrosion resistance. This behavior is attributed to the formation of a duplex Cr_2O_3/Al_2O_3 scale in the resistant alloys and the formation of single Al_2O_3 scales in the alloys that show poor corrosion resistance.

ACKNOWLEDGMENTS

The authors gratefully acknowledge the Department of Energy for providing the funds, the Materials and Molecular Research Division for providing the facilities and Mr. R.G. Miner and Mr. W. Toutolmin for their assistance in the experiments.

REFERENCES

1. R.A. Perkins, Corrosion Chemistry in Low-Oxygen Activity Atmospheres, Lockheed Research Laboratory, Palo Alto, Annual Report LMSC-D562822, June, 1977.

2. J. Stringer, Hot Corrosion in Gas Turbines, Battelle Memorial Research Institute, Columbus, Ohio, MCIC Report 72-08, 1972.

3. R. Perkins, Lockheed Research Laboratory, Quarterly Report, Palo Alto, August 1976.

4. P.L. Hemmings and R.A. Perkins, Thermodynamic Phase Stability Diagrams for the Analysis of Corrosion Reactions in Coal Gasification Atmospheres, Lockheed Research Laboratory, Palo Alto, LMSC-D558238, March 1977.

5. E.A. Gulbranson and S.A. Jansson, in Proceedings of the Symposium on High Temperature Metallic Corrosion by Sulfur and its Compounds, Foroulis, ed., Electrochem. Soc., Princeton, vol. 2A, pp. 3-54, 1970.

6. B. Gordon, W.L. Worrell and V. Nagarajan, Thermodynamic Predictions of the Behavior of Fe-Cr-Al Alloys in Coal Gasified Environments, Lawrence Berkeley Laboratory, Report LBL-7320,1977.

7. N. Birks, in Proceedings of the Symposium on Properties of High Temperature Alloys, Electrochem. Soc., Princeton, Jan. 1977.

8. R.A. Rapp, in Materials Problems and Research Opportunities in Coal Conversion, Corrosion Center, Ohio State University, Vol. II, April 1974.

9. R.A. Perkins and M.S. Bhat, Sulfidation Resistant Alloy for Coal Gasification Service, Lockheed Research Laboratory Annual Report, Palo Alto, May 1977.

10. R.G. Miner, M.S. thesis, Department of Materials Science, University of California, Berkeley, to be published.

11. F.S. Pettit, Materials Engineering and Research Laboratory, Pratt and Whitney Aircraft, Connecticut, private communication.

12. F.H. Stott et al., Oxidation of Metals, Vol. 3, No. 2, p. 103, March 1971.

13. Handbook of Stainless Steels, Peckner, D., and Bernstein, I.M., eds. (McGraw-Hill Book Company, New York, 1977), p. 17.

Table 1. Coal gasification atmosphere (mol fraction).

	Raw Gas	Equilibrated	
		1 atm	68 atm
H_2	0.24	0.366	0.335
H_2O	0.39	0.305	0.325
CO	0.18	0.206	0.191
CO_2	0.12	0.109	0.118
CH_4	5×10^{-2}	5.1×10^{-6}	1.6×10^{-2}
H_2S	1×10^{-2}	8.8×10^{-3}	9.1×10^{-3}
NH_3	1×10^{-2}	2.2×10^{-6}	1.3×10^{-4}
COS	-	1.6×10^{-4}	1.7×10^{-4}
S_2	-	2.4×10^{-6}	4.5×10^{-8}
O_2	-	1.8×10^{-9}	2.0×10^{-17}
P_{O_2} - atm		9.9×10^{-16}	1.34×10^{-15}
P_{S_2} - atm		2.4×10^{-6}	3.06×10^{-6}
a_C		3.11×10^{-3}	1.68×10^{-1}

Table 2. The nominal and actual compositions of investigated alloys.

Alloy No.	Nominal Composition in wt%	Actual Composition in wt%			
		Fe	Cr	Si	Al
1	Fe-18Cr-0.5Si	Bal	17.91	0.40	-
2	Fe-18Cr-1.0Si	Bal	17.84	0.90	-
3	Fe-18Cr-1.5Si	Bal	17.78	1.31	-
4	Fe-18Cr-2.0Si	Bal	17.93	1.91	-
5	Fe-18Cr-1.0Al	Bal	17.91	-	0.86
6	Fe-18Cr-3.0Al	Bal	17.56	-	2.56
7	Fe-18Cr-5.0Al	Bal	17.74	-	4.34
8	Fe-18Cr-7.0Al	Bal	17.64	-	6.64
9	Fe-10Al	Bal	-	-	9.29
10	Fe-10Al-5Cr	Bal	4.91	-	9.03
11	Fe-10Al-10Cr	Bal	14.64	-	9.21
12	Fe-10Al-15Cr	Bal	16.83	-	8.76

Table 3. The weight gain/uit area data for all 12 alloys corroded without preoxidation.

Alloy No.	Weight Gain/Unit Area mg/cm^2			
	1 Day	2 Days	3 Days	5 Days
1	1.3243	209.15	237.312	205.630
	1.4193	211.637	-	229.373
2	1.2011	32.15	107.583	207.914
	35.661	53.213	214.946	151.410
3	1.4123	0.329	209.459	189.426
	25.646	0.1201	185.393	49.240
4	1.2566	0.824	107.606	13.023
	0.509	0.2179	-	18.736
5	1.0705	9.49	86.494	215.623
	1.038	26.13	12.329	205.604
6	1.1803	7.96	-0.974	6.521
	-	6.361	1.795	1.0412
7	1.0157	8.49	-0.323	4.036
	0.855	4.706	-1.022	9.1132
8	1.1293	7.79	1.178	9.597
	1.413	14.734	-0.729	16.925
9	1.9964	22.735	192.227	201.901
	2.171	155.69	-	225.893
10	0.8540	1.086	63.372	2.064
	173.738	0.9097	85.193	7.308
11	1.0650	0.6887	71.510	245.825
	1.765	6.871	6.580	224.004
12	1.1866	36.62	122.993	177.352
	1.702	28.021	-	123.717

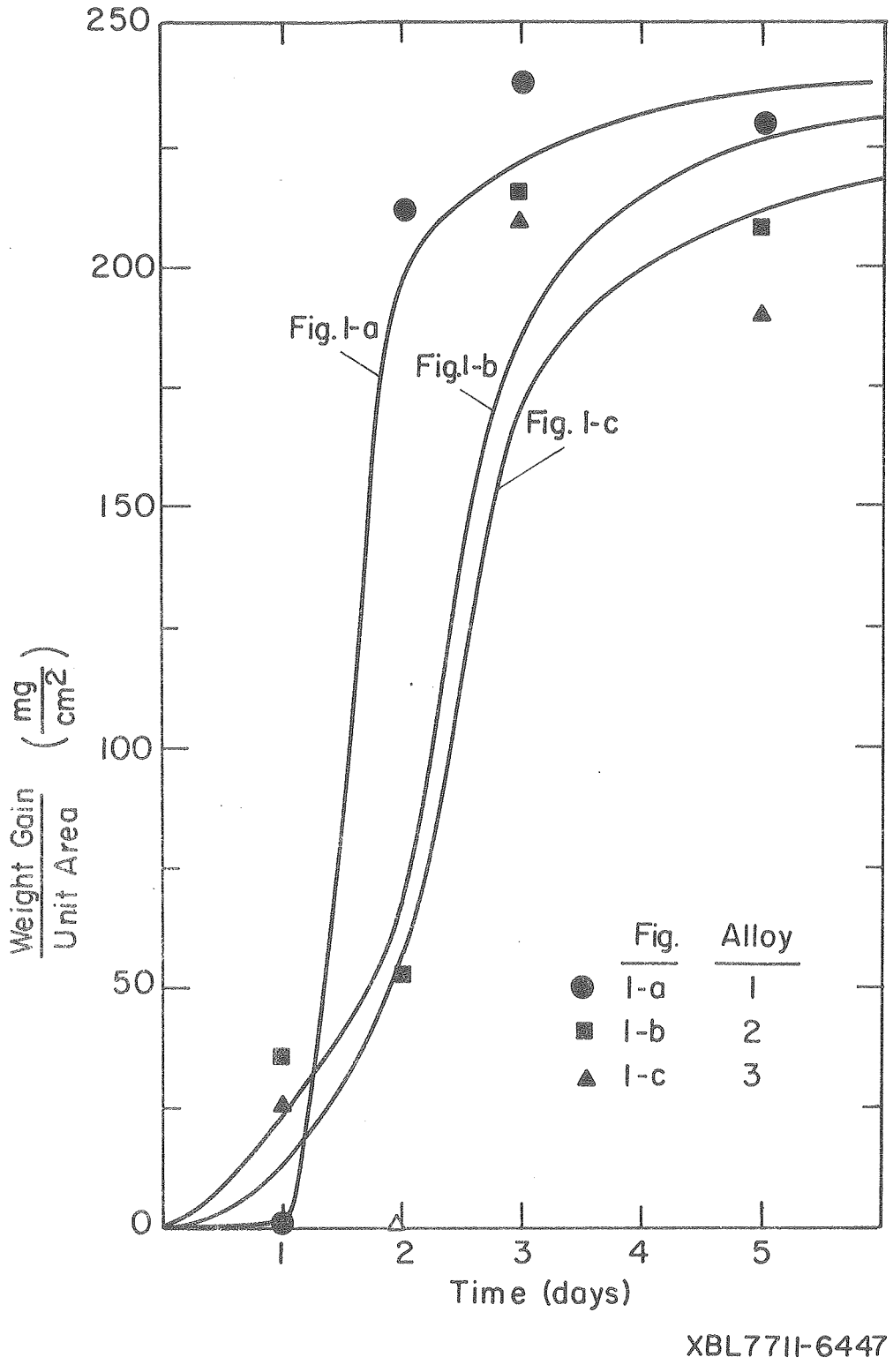

Fig. 1. (abc) The weight gain/unit area data for alloys 1, 2, and 3 plotted against time. The plots are based on data obtained from specimens corroded for 1, 2, 3, and 5 days separately. The curves are only qualitative and not quantitative.

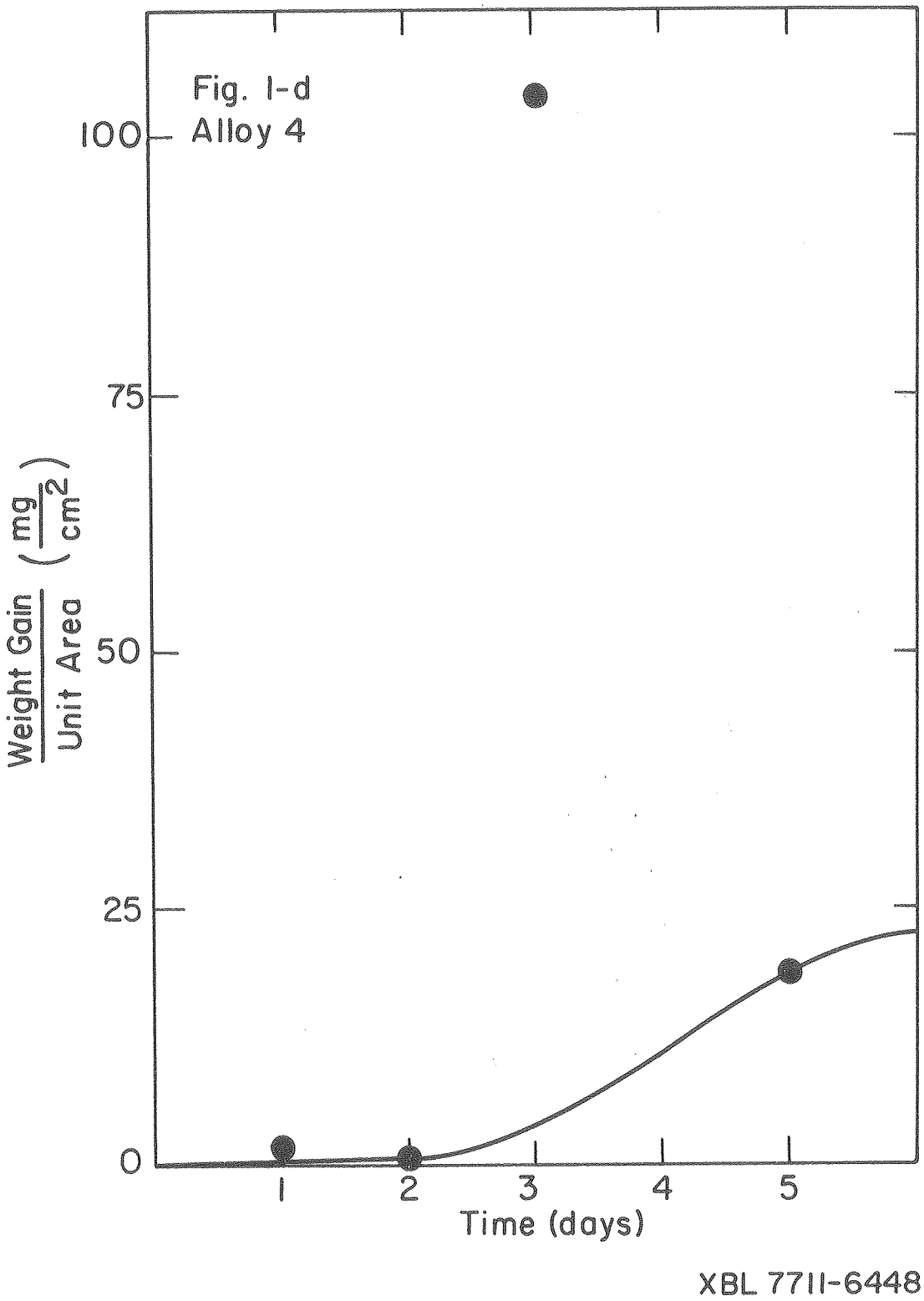

Fig. 1. (d) The weight gain/unit area data for alloy 4 plotted against time. The alloy shows very little corrosion up to 2 days, but then starts to corrode. Note that weight gain after 3 days is very high compared to the weight gain after 5 days.

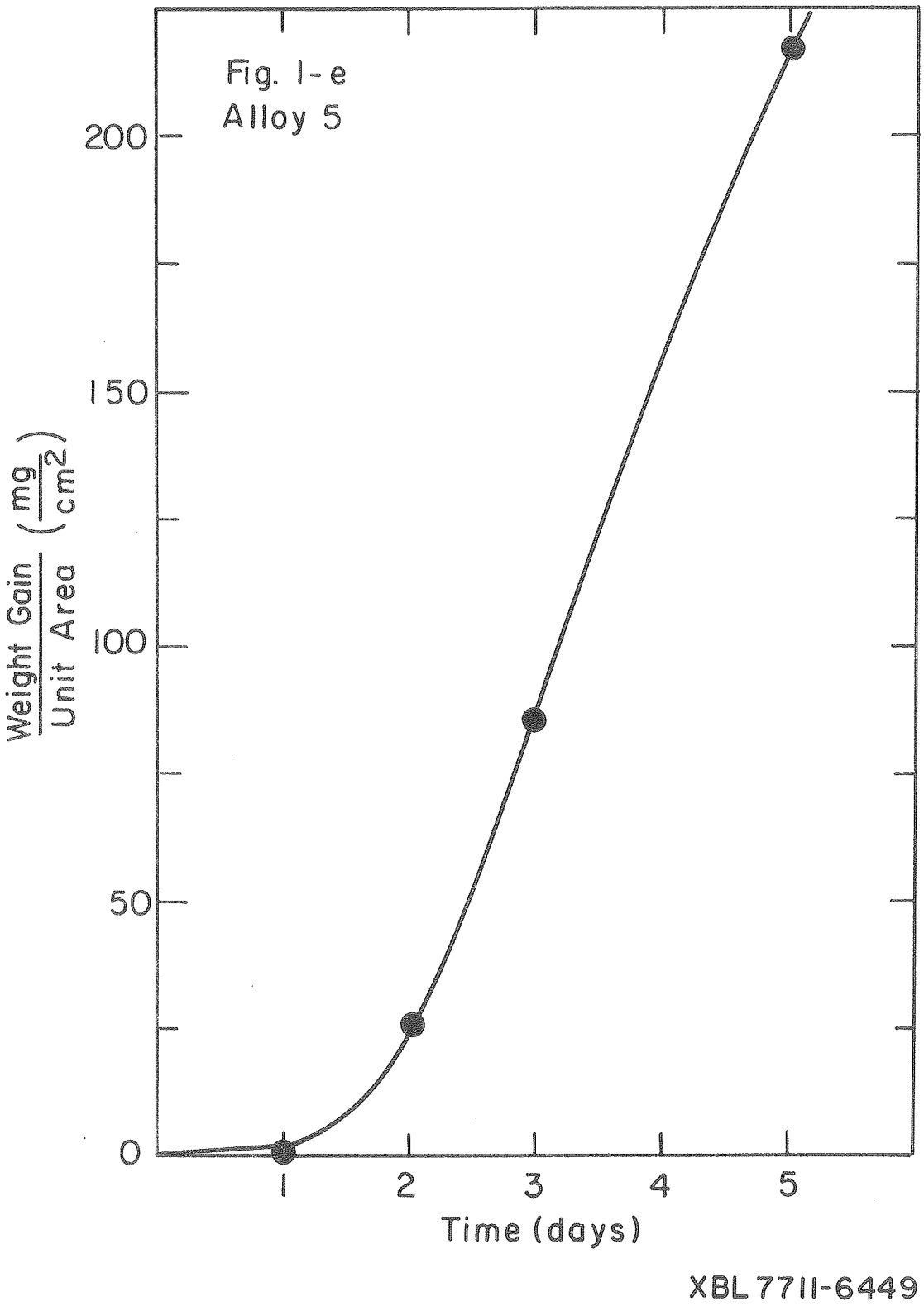

Fig. 1. (e) The weight gain/unit area data for alloy 5 plotted against time. Note the accelerated corrosion after 2 days.

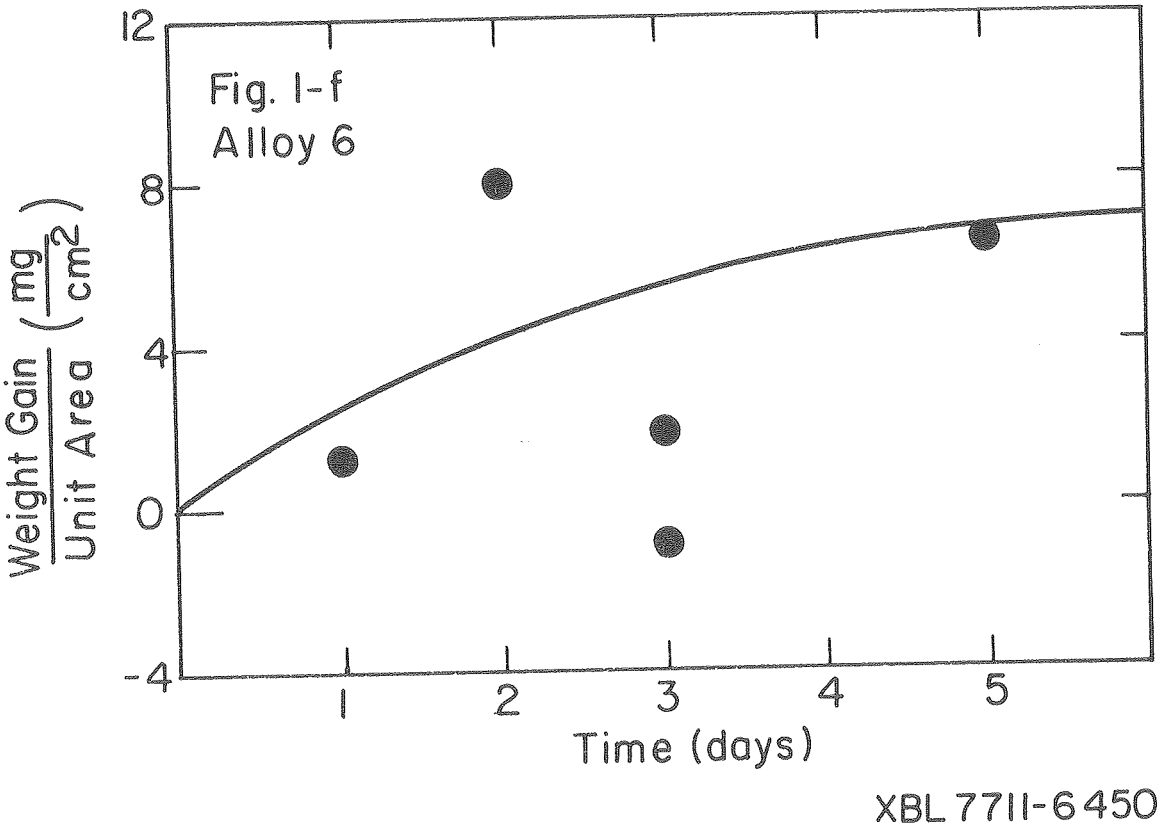

Fig. 1. (f) The weight gain/unit area data for alloy 6 plotted against time. Note the negative weight gain after 3 days. This negative weight gain is due to scale spallation.

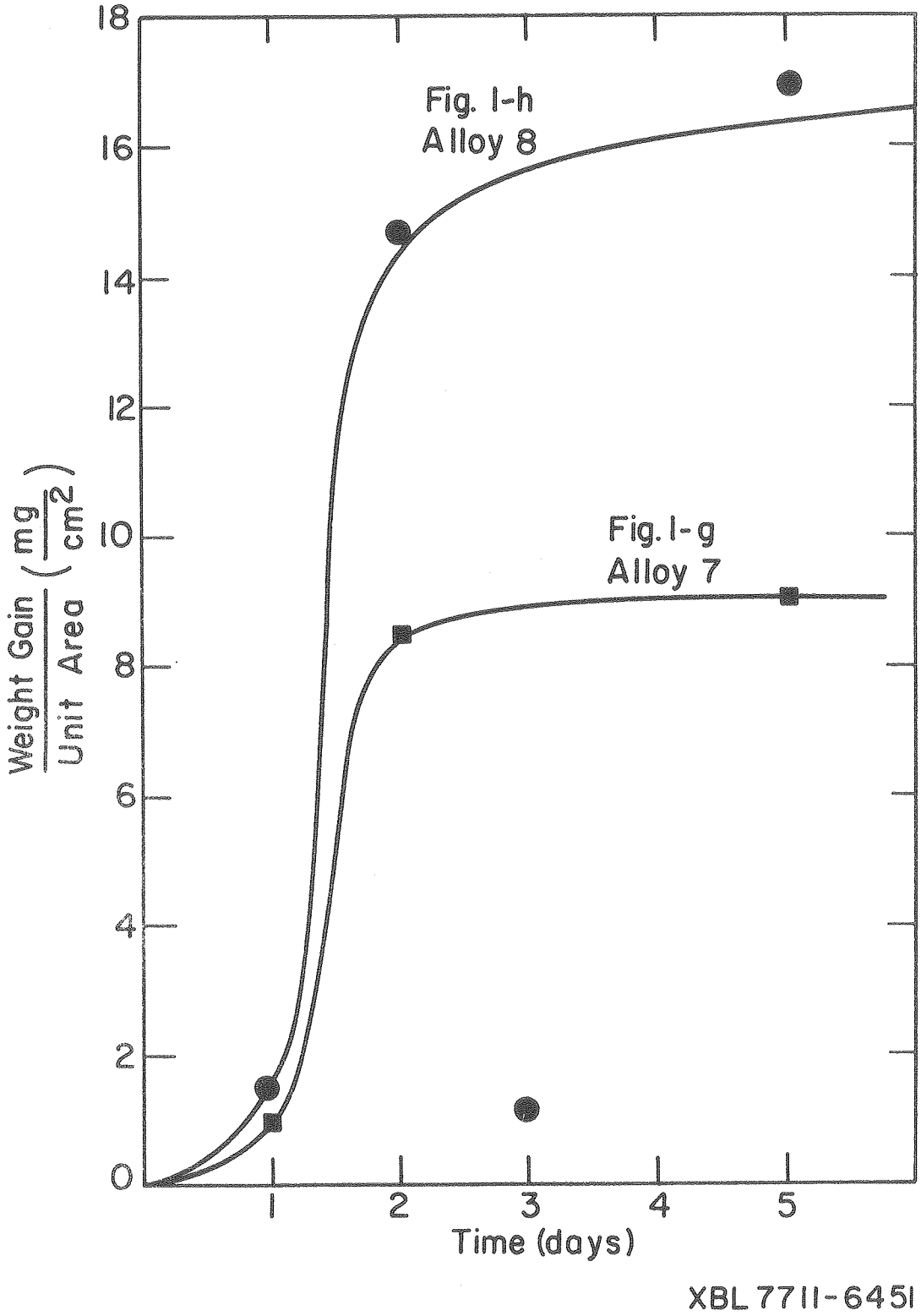

Fig. 1. (gh) The weight gain/unit area data for alloys 7 and 8 plotted against time. Although the overall weight gain for alloy 8 after 5 days of corrosion is only 17 mg/cm^2, the specimen has suffered severe local corrosion.

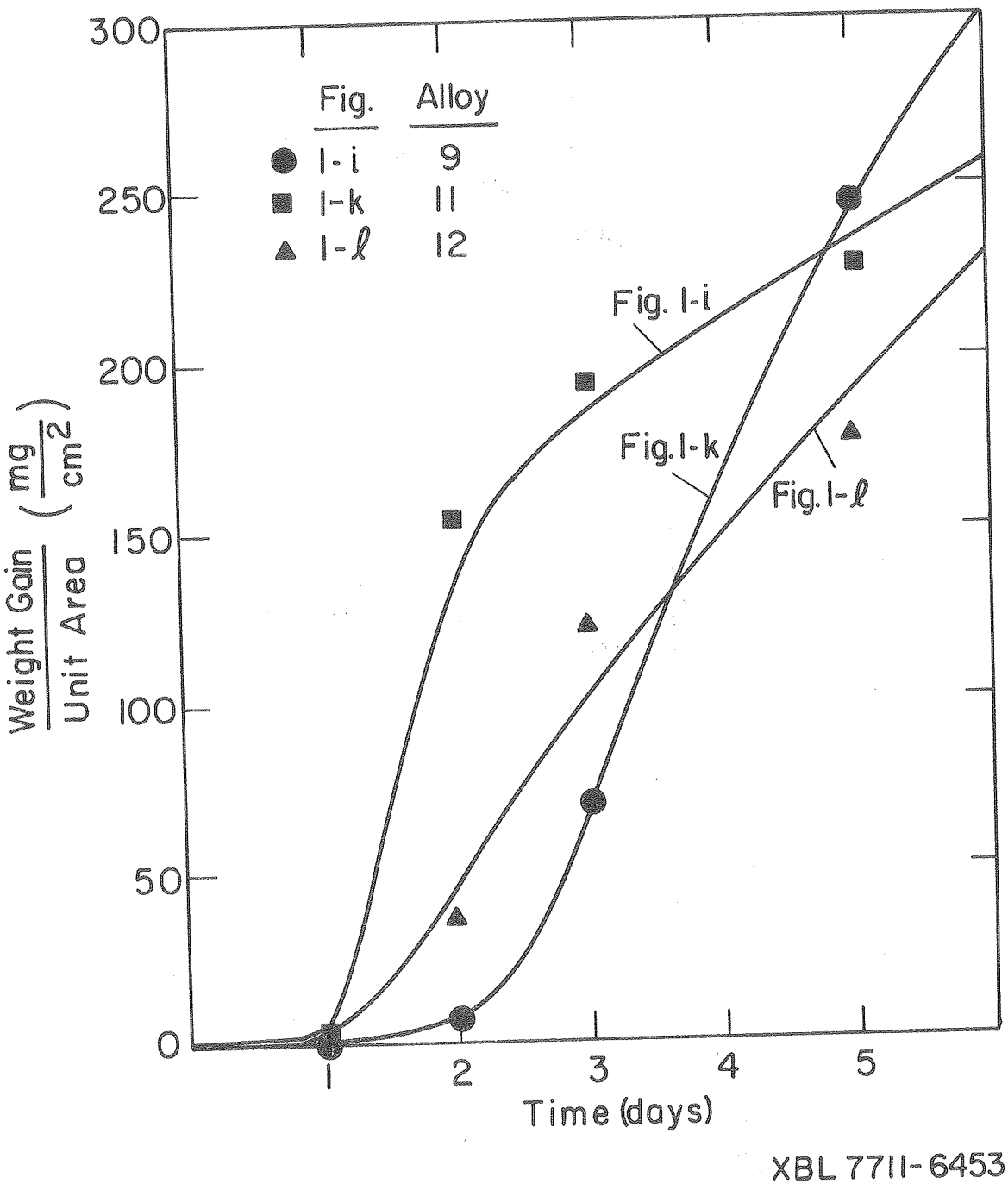

Fig. 1. (ikl) The weight gain/unit area data for alloys 9, 11, and 12, corroded for 1, 2, 3, and 5 days, are plotted against time. No importance should be attached to the shape of the curves, which are only meant to show the corrosion behavior qualitatively.

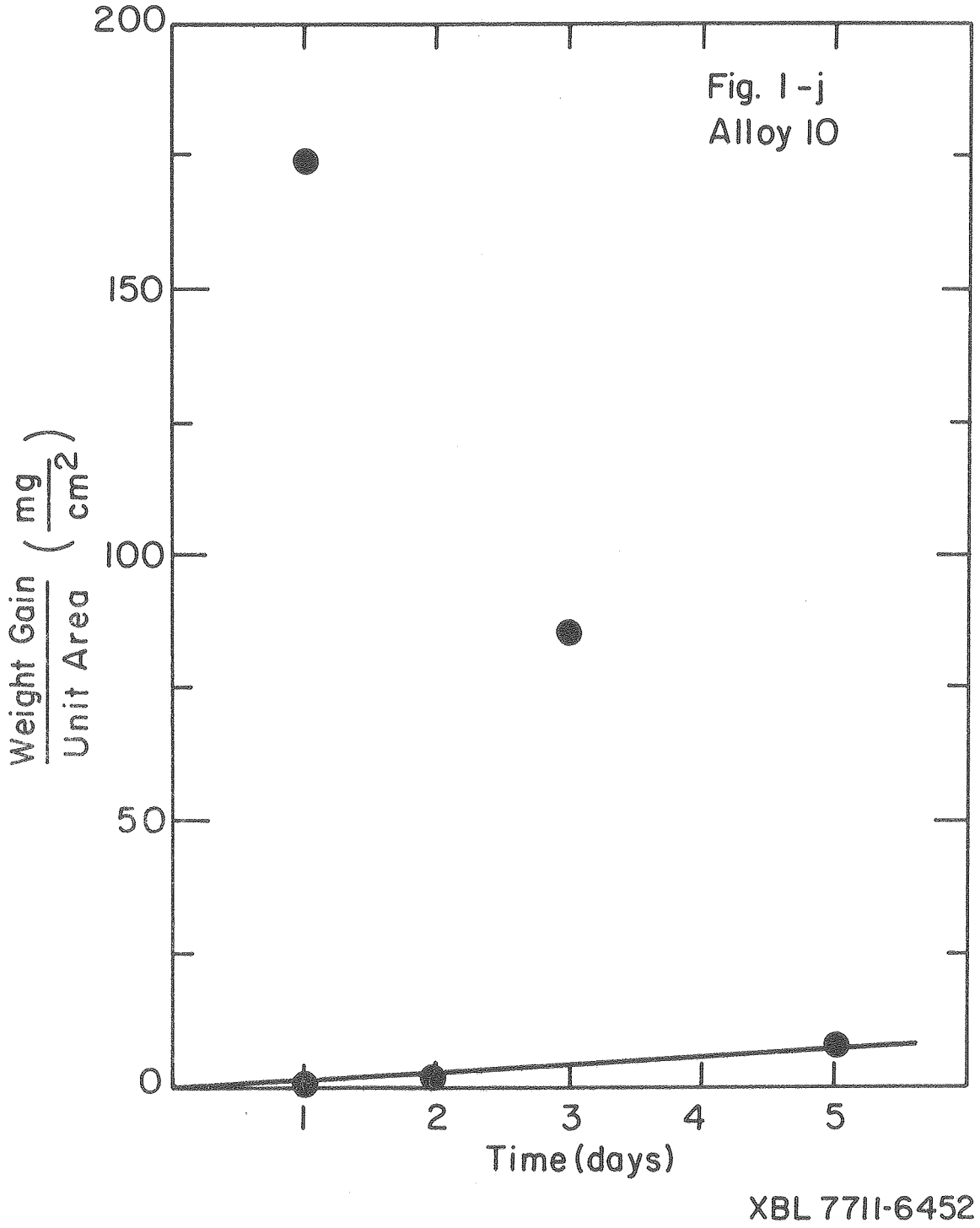

Fig. 1. (j) The weight gain/unit area data for alloy 10. The data show considerable scatter.

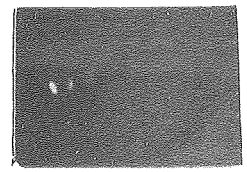

1 DAY

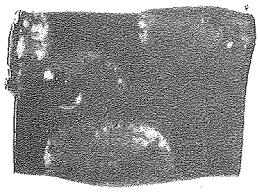

2 DAYS

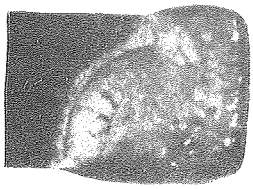

3 DAYS

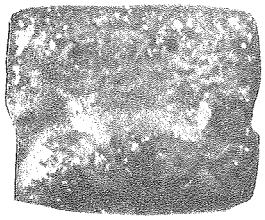

5 DAYS

XBB 778-8156

Fig. 2. The external appearances of alloy 2 specimens corroded for 1, 2, 3, and 5 days. The corrosion starts from edges and corners, increasing its area of coverage with increase in time.

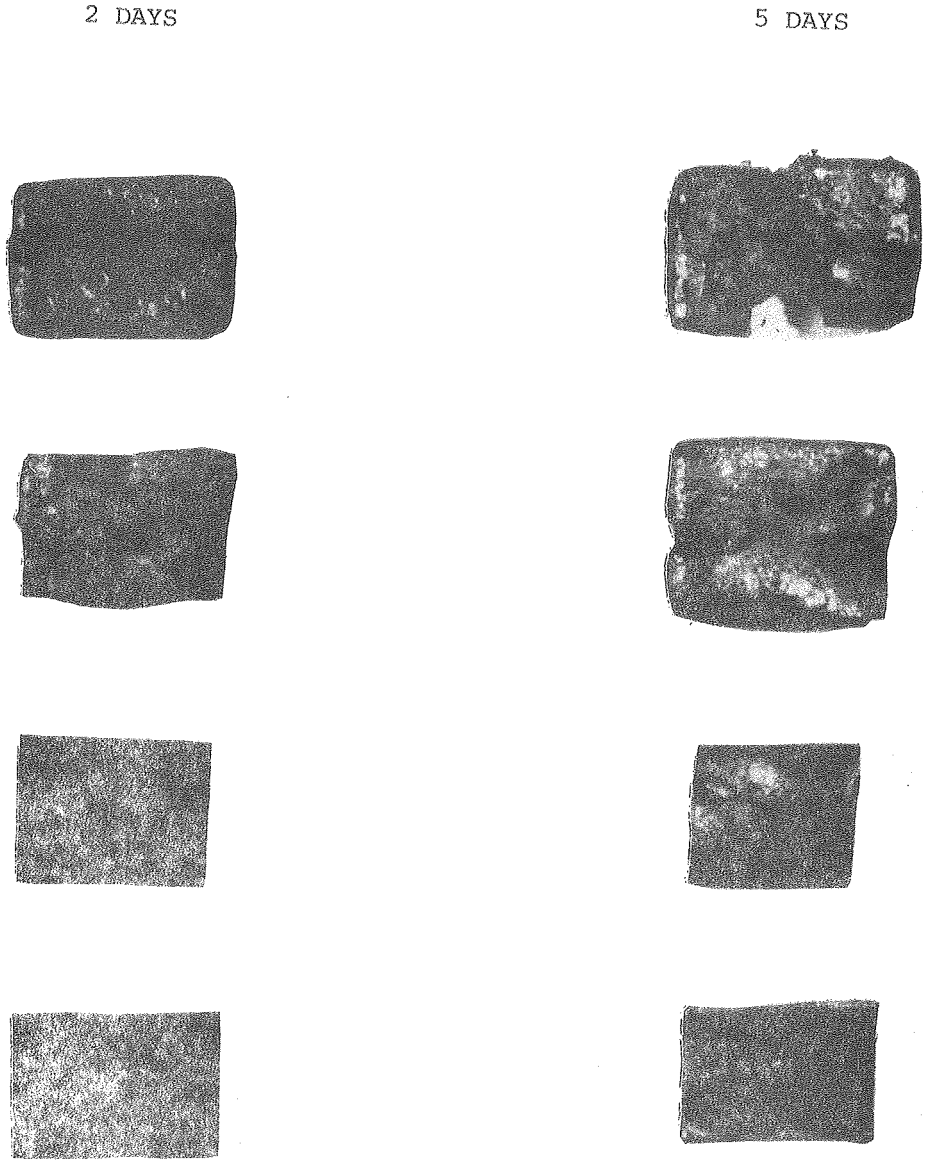

XBB 778-8158

Fig. 3. The external appearances of alloys 1, 2, 3, and 4 corroded for 2 and 5 days. Rows 1 to 4 from the top represent alloys 1 to 4 respectively.

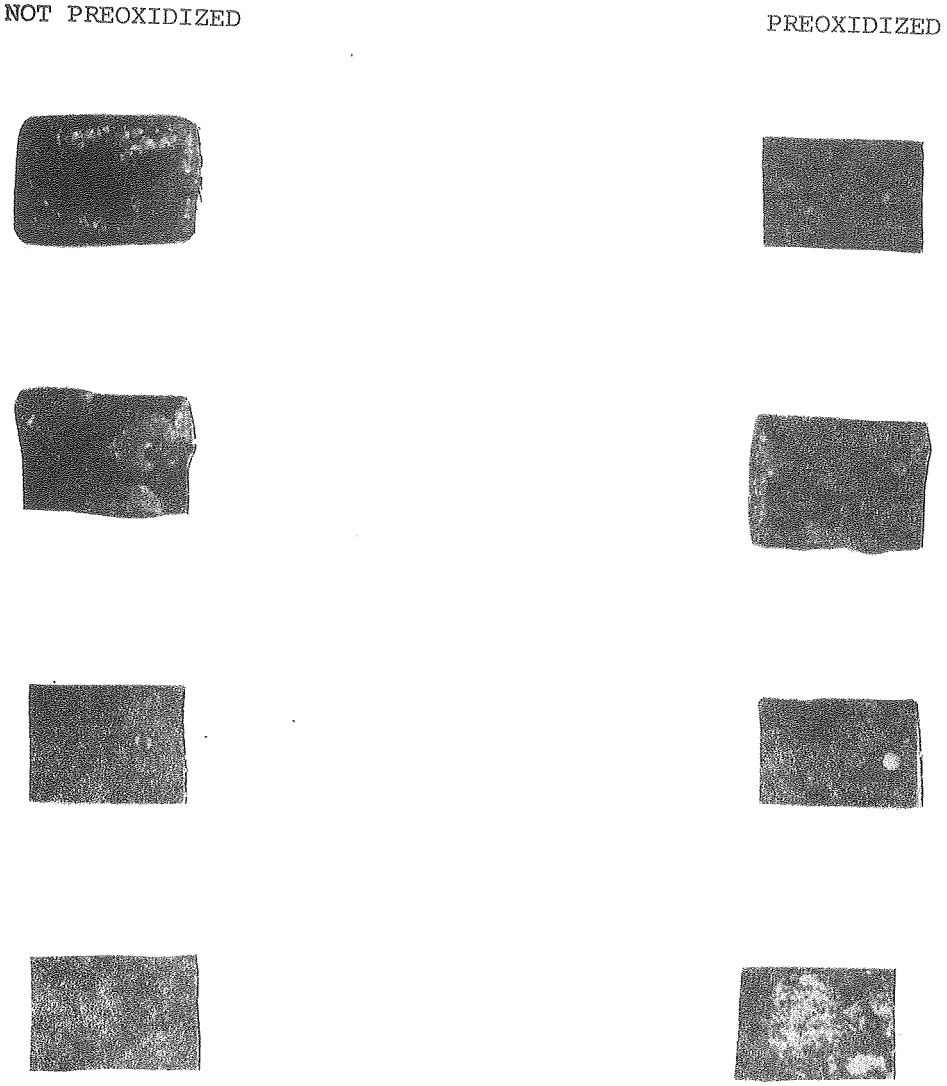

Fig. 4. (a) The external appearances of alloys 1 to 4 corroded for 2 days, both without and with the preoxidation treatment. Rows 1 to 4 from the top represent alloys 1 to 4 respectively.

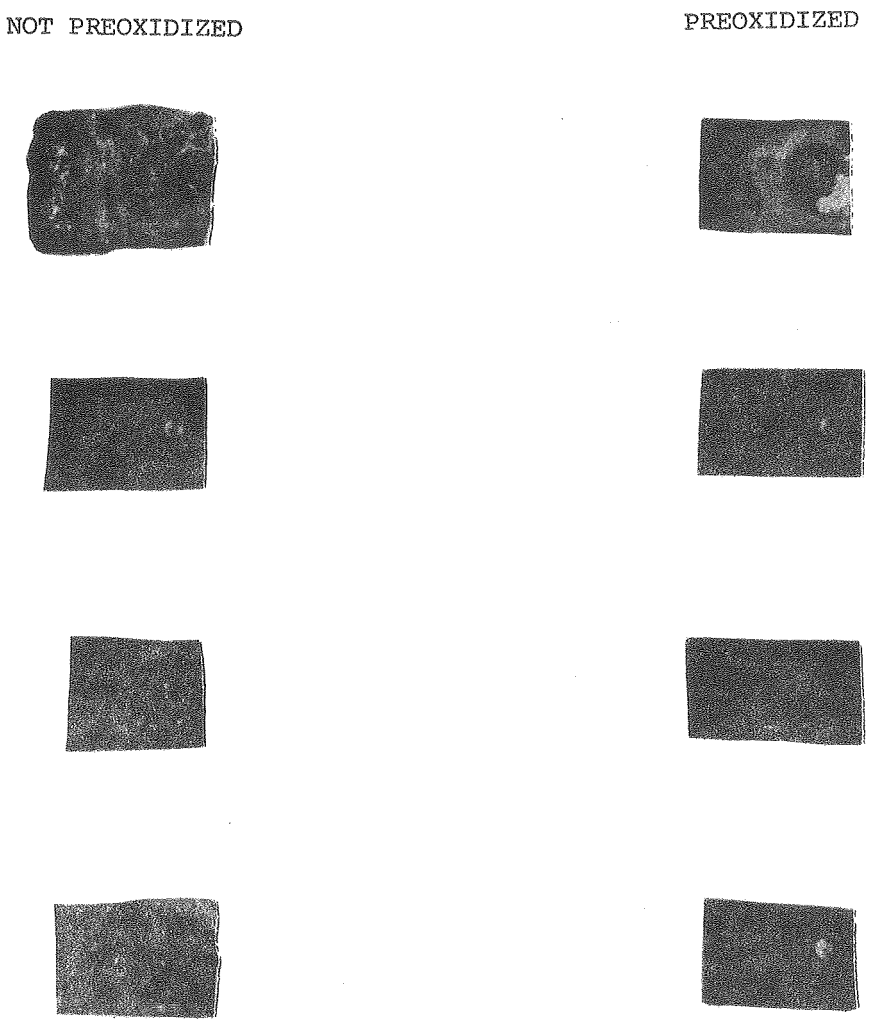

XBB 778-8876

Fig. 4. (b) The external appearances of alloys 9 to 12 corroded for 2 days, both without and with the preoxidation treatment. Rows 1 to 4 from the top represent alloys 9 to 12 respectively.

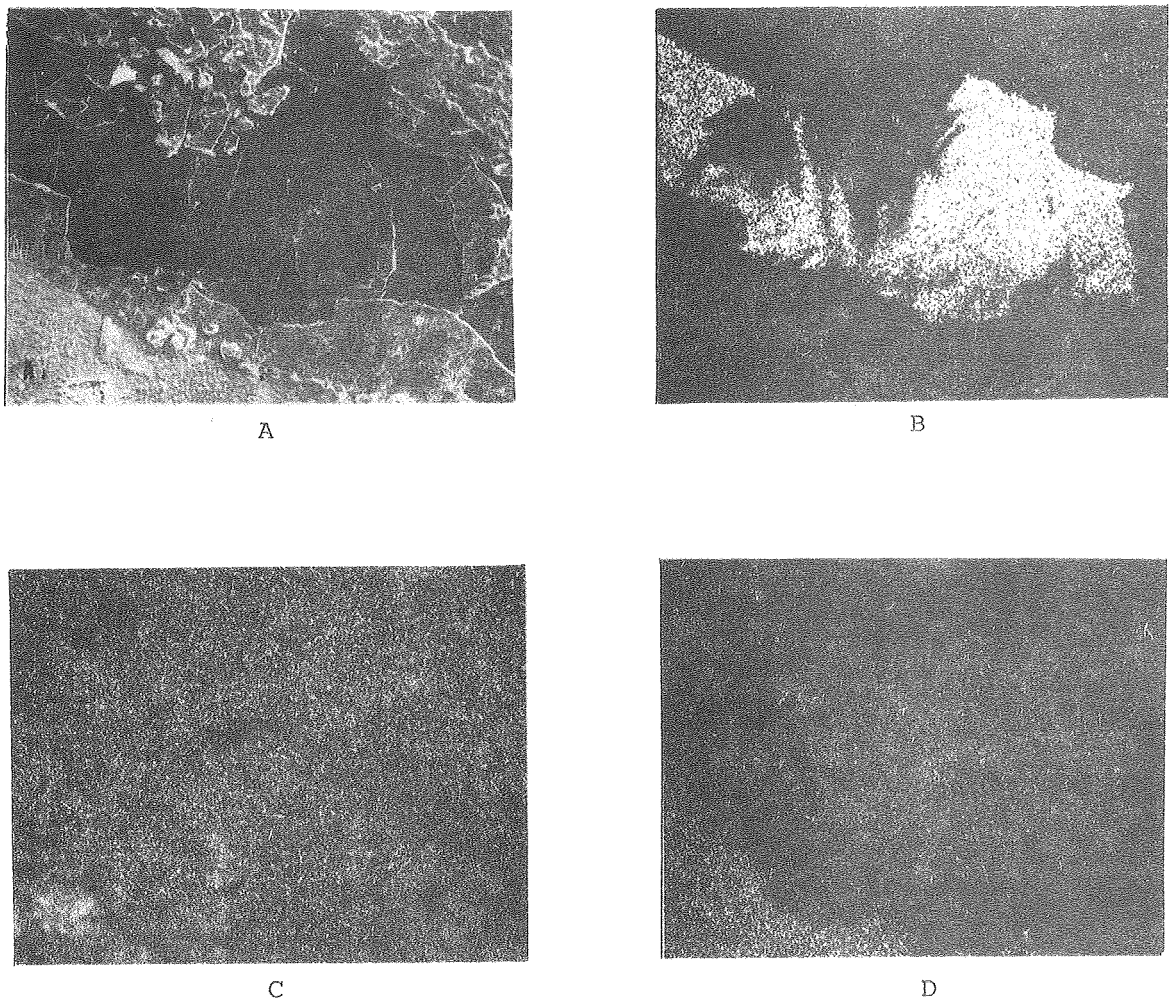

XBB 781-180

Fig. 5. The surface of a specimen of Fe-18Cr-1.0Si alloy corroded for 1 day. The area marked "A" is a secondary electron image of the surface scale. "B" is an x-ray map for S, "C" is an x-ray map for Fe, and "D" is an x-ray map for Cr. The figure shows the formation of sulfide within one day of corrosion, which results in the cracking of the outer Cr_2O_3 scale. The figure is magnified 200X.

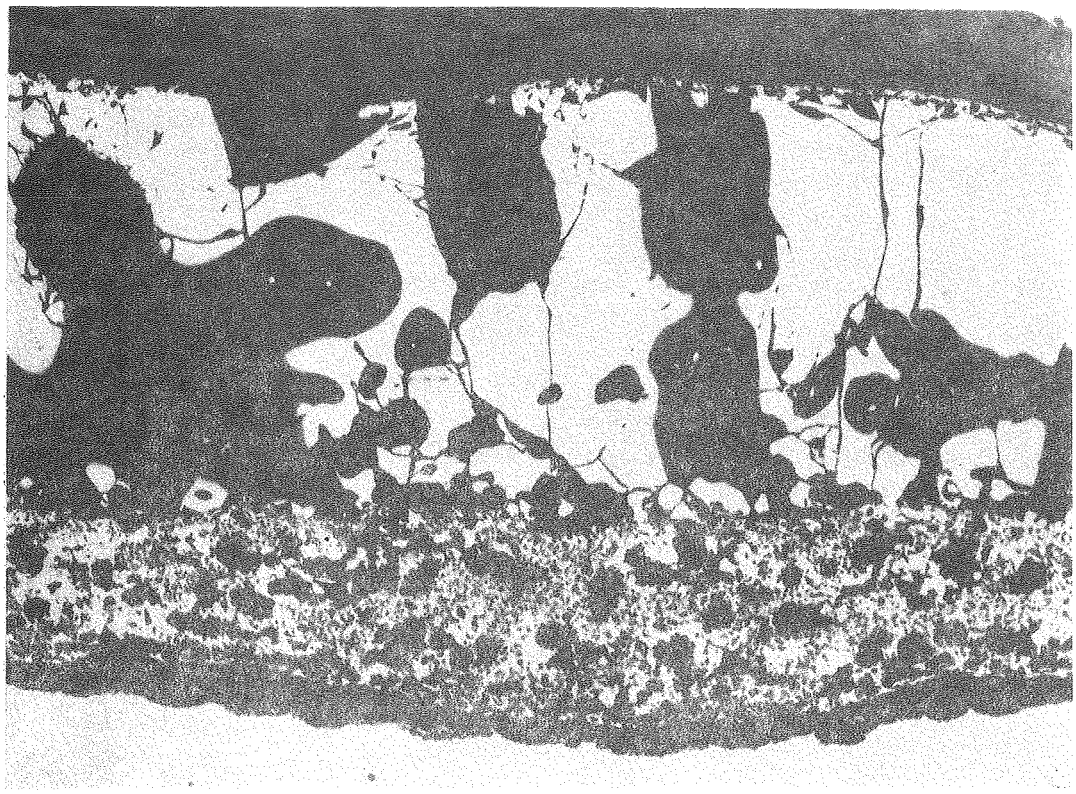

XBB 781-189

Fig. 6. The optical micrograph of the cross section of an Fe-18Cr-0.5Si alloy specimen corroded for 1 day. The outermost layer is iron-rich sulfide. The inner layer, marked "B", consists of a mixture of Cr_2O_3 and the sulfide. The figure is magnified at 128X.

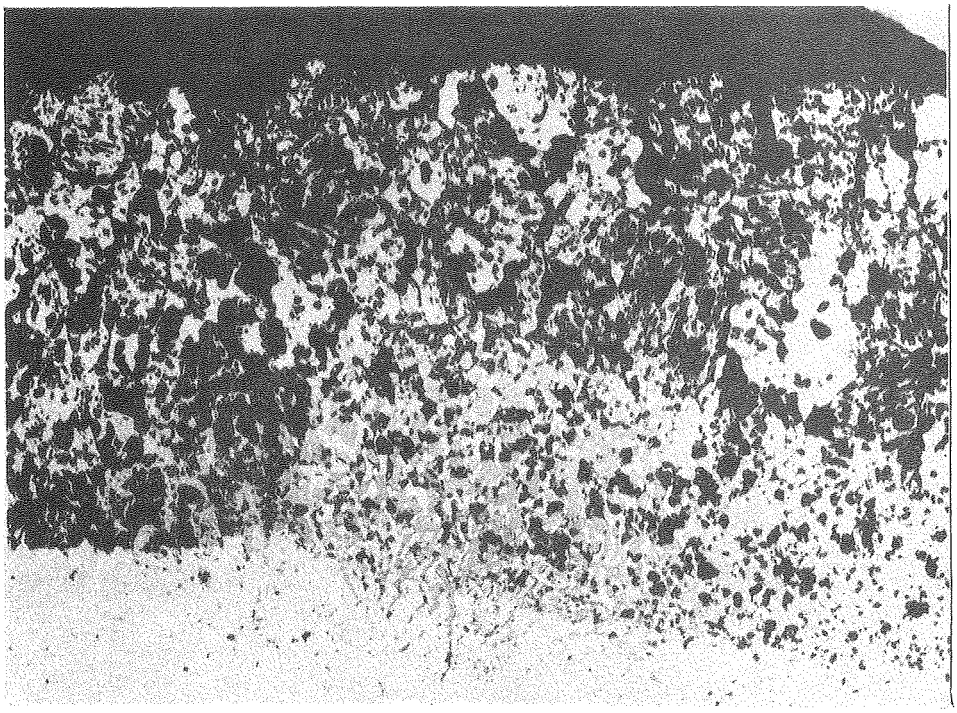

XBB 781-188

Fig. 7. The optical micrograph, magnified 160X, of the cross section of an Fe-18Cr-0.5Si specimen corroded for 2 days. The outer, iron-rich sulfide has spalled off. The micrograph shows only the inner scale. The light-colored globular precipitates near the unreacted metal are chromium sulfides.

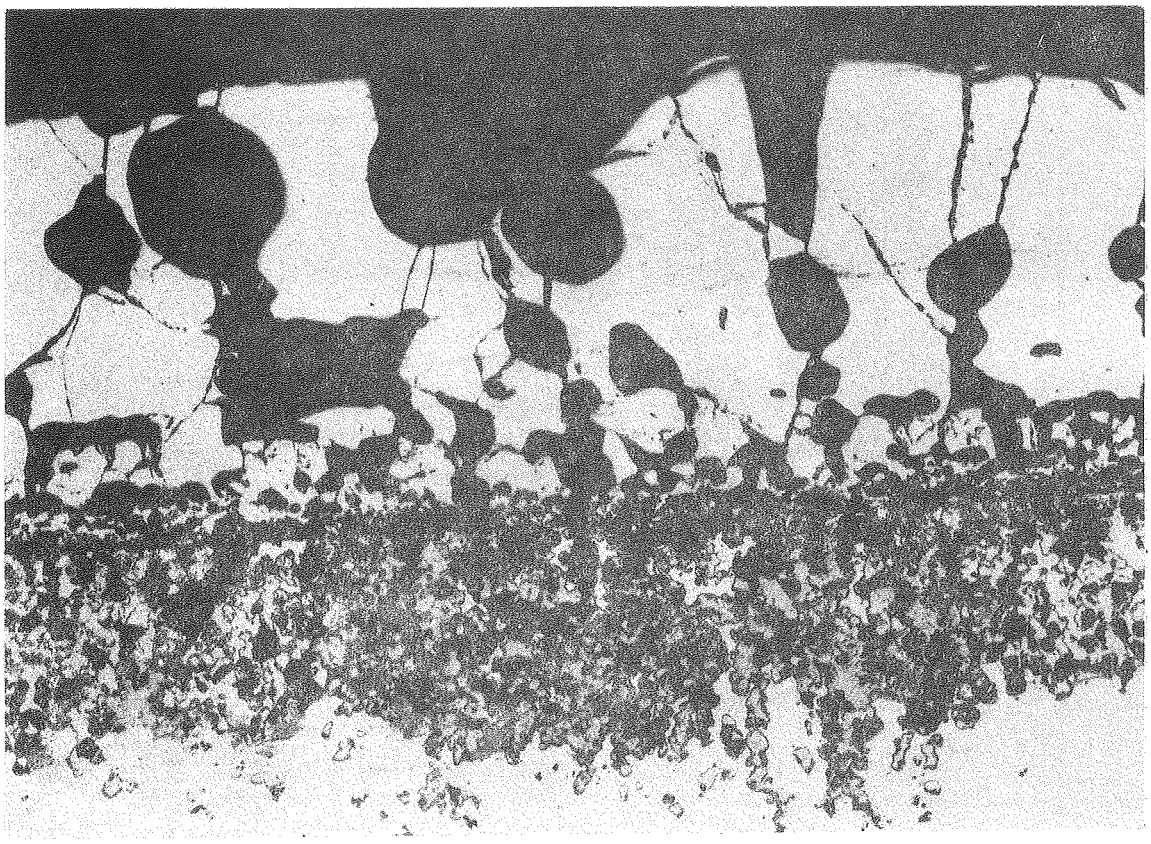

XBB 781-187

Fig. 8. The optical micrograph, magnified 88X, of the cross section of the Fe-18Cr-2Si alloy corroded for 3 days. The outer scale is the iron-rich sulfide. The inner scale consists of Cr_2O_3, chromium-rich sulfides and unreacted metal.

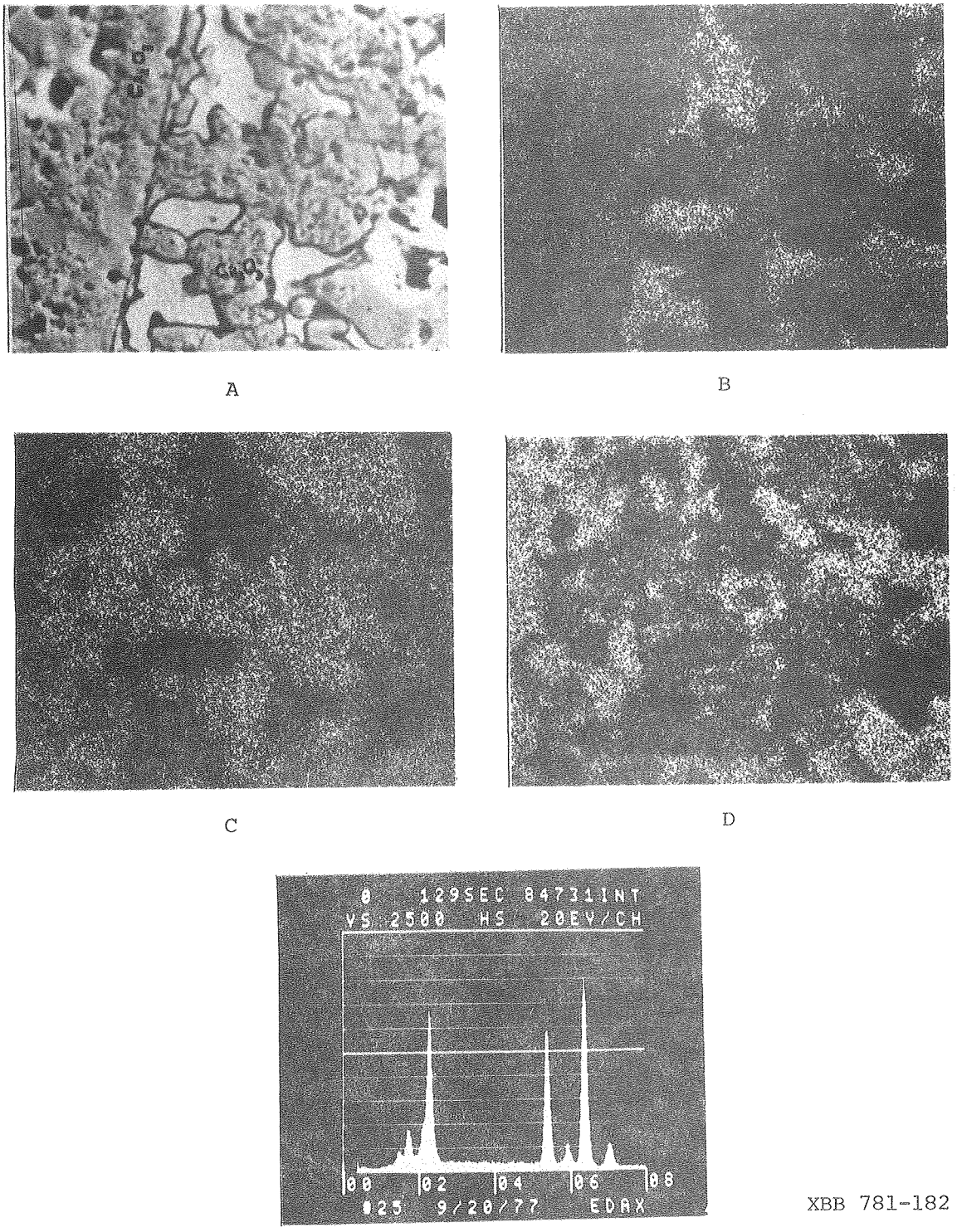

Fig. 9. An area, magnified 250X, of the inner scale of an Fe-18Cr-2Si alloy specimen corroded for 3 days. "A" is the secondary electron image. "B" shows the x-ray map for Fe. The iron-rich areas are unreacted metal. "C" is the x-ray map for Cr, and "D" is the x-ray map for S. The Cr and S maps show areas rich in Cr which have no S. These areas are Cr_2O_3 and are marked in the micrograph. The EDAX peaks of a sulfide area show it to be a Fe-Cr complex sulfide.

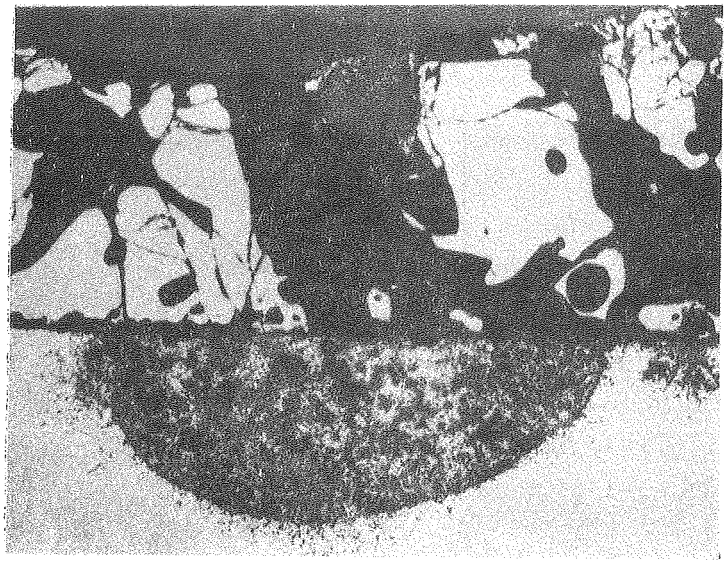

A

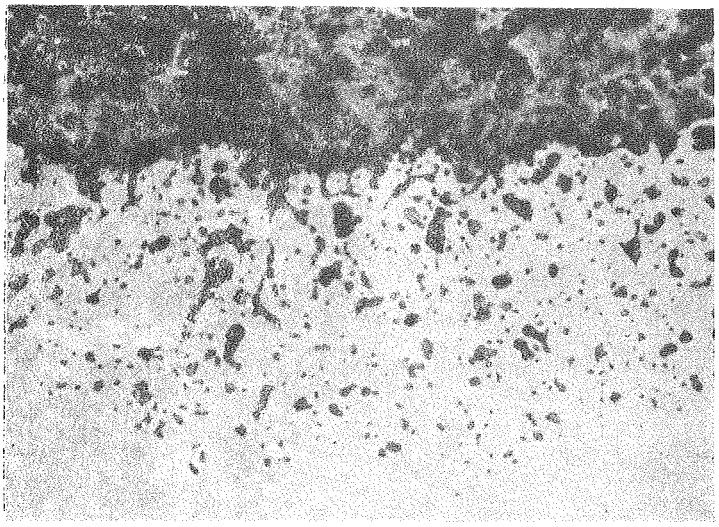

B

XBB 781-181

Fig. 10. The optical micrograph of a specimen of Fe-18Cr-1Al alloy corroded for 3 days. "A" is the outer scale, magnified 40X, which is iron-rich sulfide. "B" is the inner scale, magnified 320X, which consists of a mixture of Cr_2O_3 and Cr-rich sulfides.

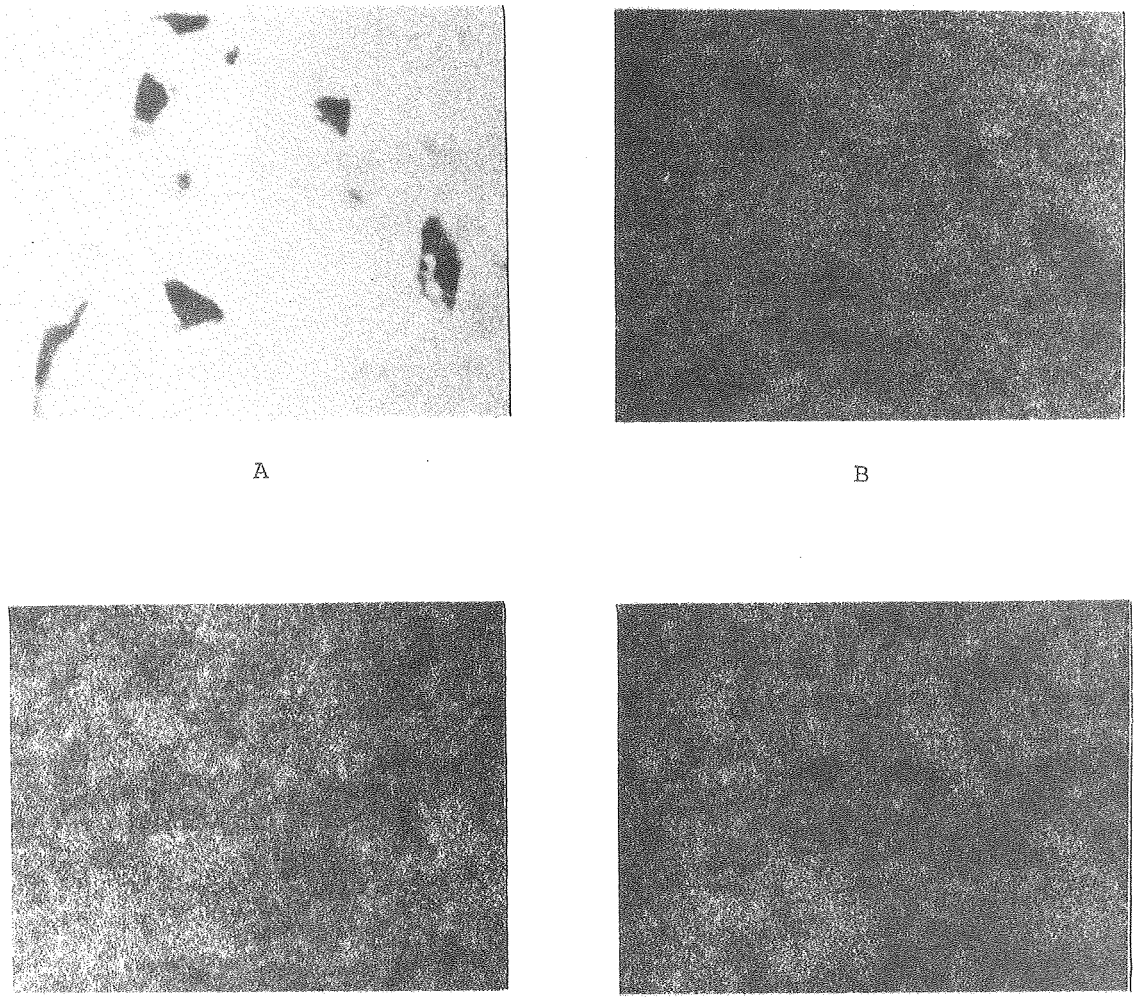

Fig. 11. A specimen of Fe-18Cr-1Al alloy, magnified 500X, corroded for 3 days. The internal precipitates, shown in a secondary electron image in "A", are analyzed. The x-ray maps for Fe, Cr, and S, which are "B", "C", and "D" respectively, show that the internal precipitates are Cr-rich sulfides.

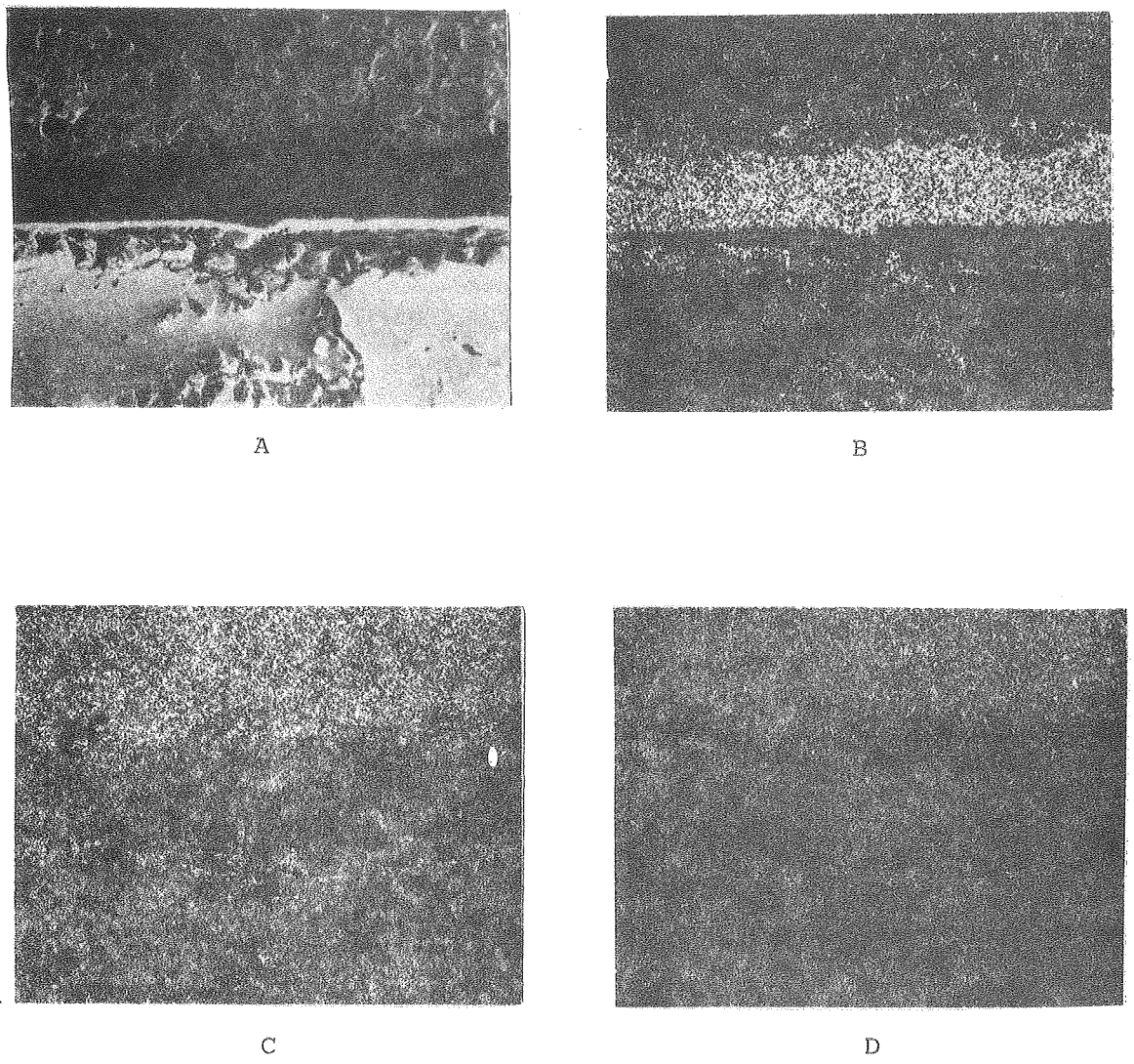

Fig. 12. A specimen of Fe-18Cr-7Al alloy, magnified 150X, corroded for 5 days. "A" is the secondary electron image, "B" is the x-ray map for Al, "C" is the x-ray map for S, and "D" is the x-ray map for Cr. The topmost layer consists of Fe-Cr sulfide. The x ray for Al reveals a thick band ($\simeq$75 microns) of Al_2O_3. Precipitates of Al_2O_3 are also seen in the topmost layer and within the alloy. A layer of Cr-rich sulfide is also seen at the scale/alloy interface.

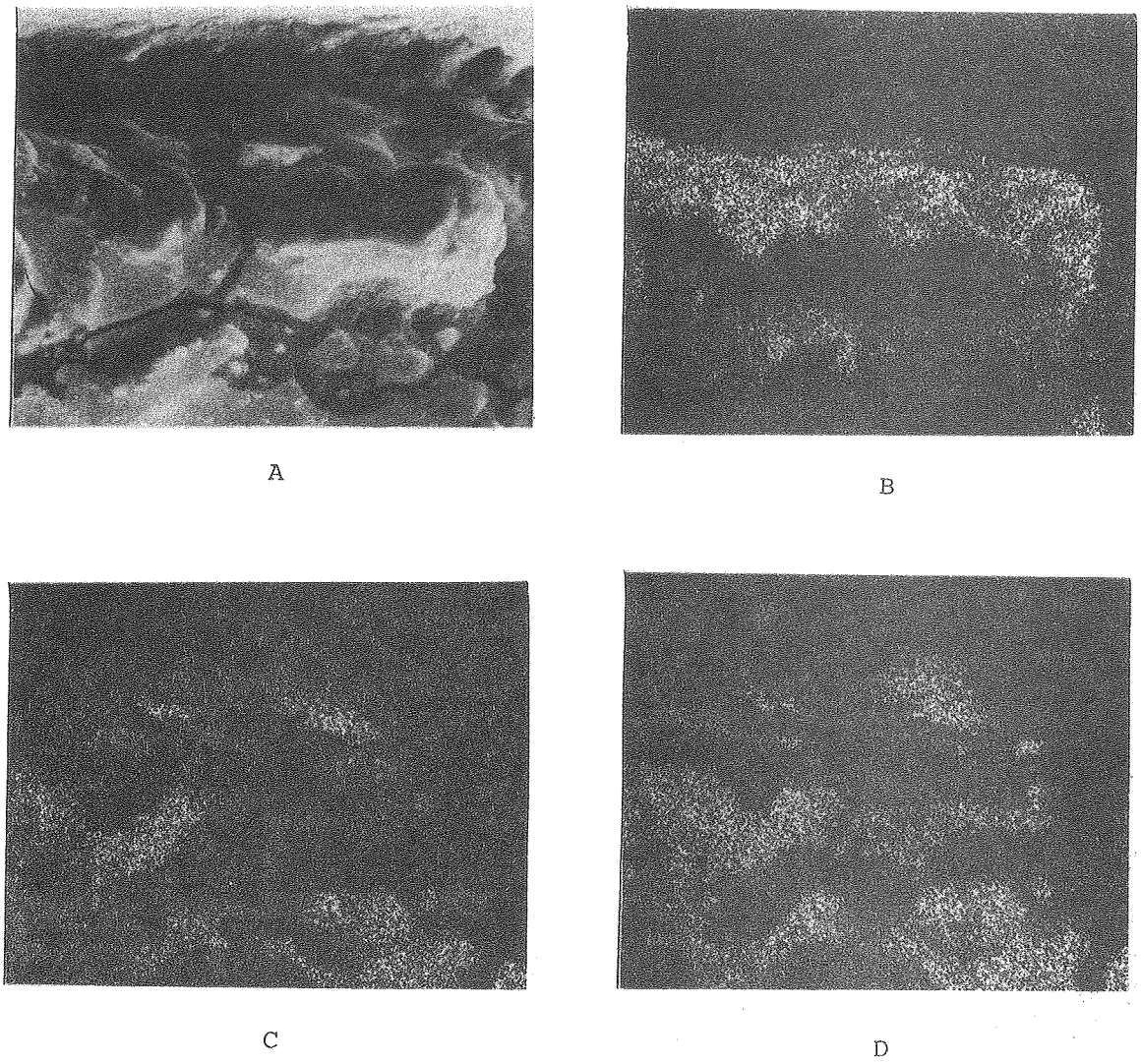

Fig. 13. The scale/alloy interface of Figure 12 at a high magnification (1100X). "A" is the secondary electron, "B" is an x-ray map for Al, "C" is an x-ray map for S, and "D" is an x-ray map for Cr. The micrograph reveals not only Cr-rich sulfides but also Cr oxides. The Al map shows Al_2O_3 both above and beneath the sulfides.

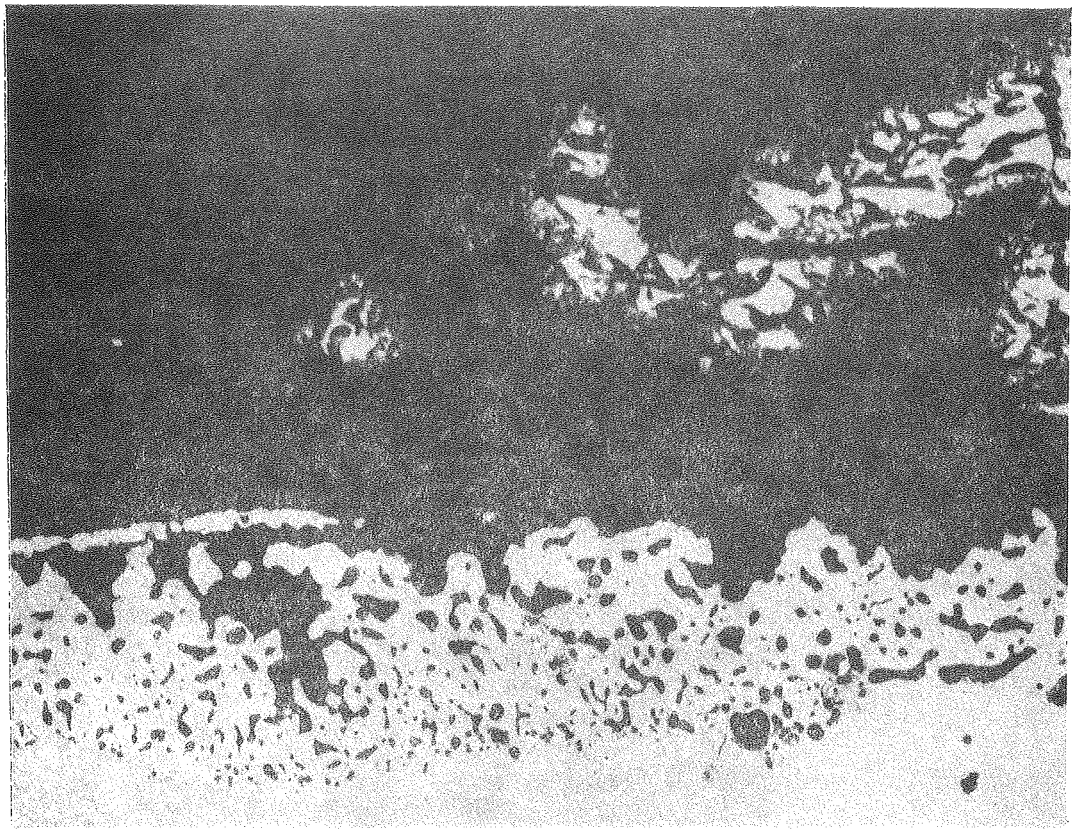

XBB 781-186

Fig. 14. The optical micrograph, magnified 240X, of the cross section of an Fe-10Al alloy corroded for 2 days. Most of the outer iron-sulfide scale has spalled off and only a small portion of it is seen in the micrograph. The dark precipitates in the alloy are mainly Al_2O_3 (smaller precipitates) and voids (larger precipitates).

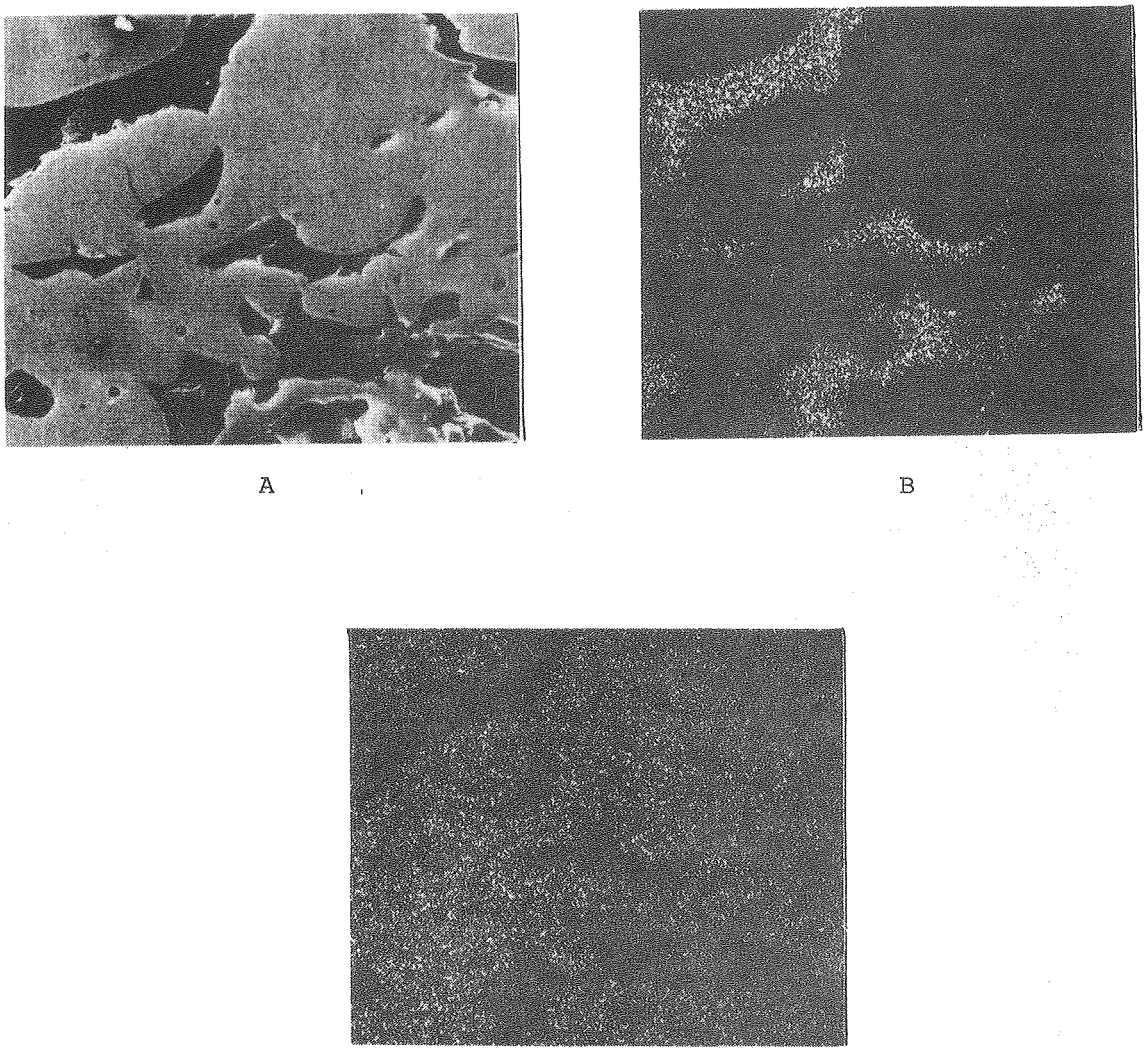

A B C

XBB 781-185

Fig. 15. The internal precipitates of the area shown in Figure 14, magnified 750X. The Al and Fe maps, "B" and "C", show that the internal precipitates are Al rich. No sulfur was detected and hence the precipitates are Al_2O_3.

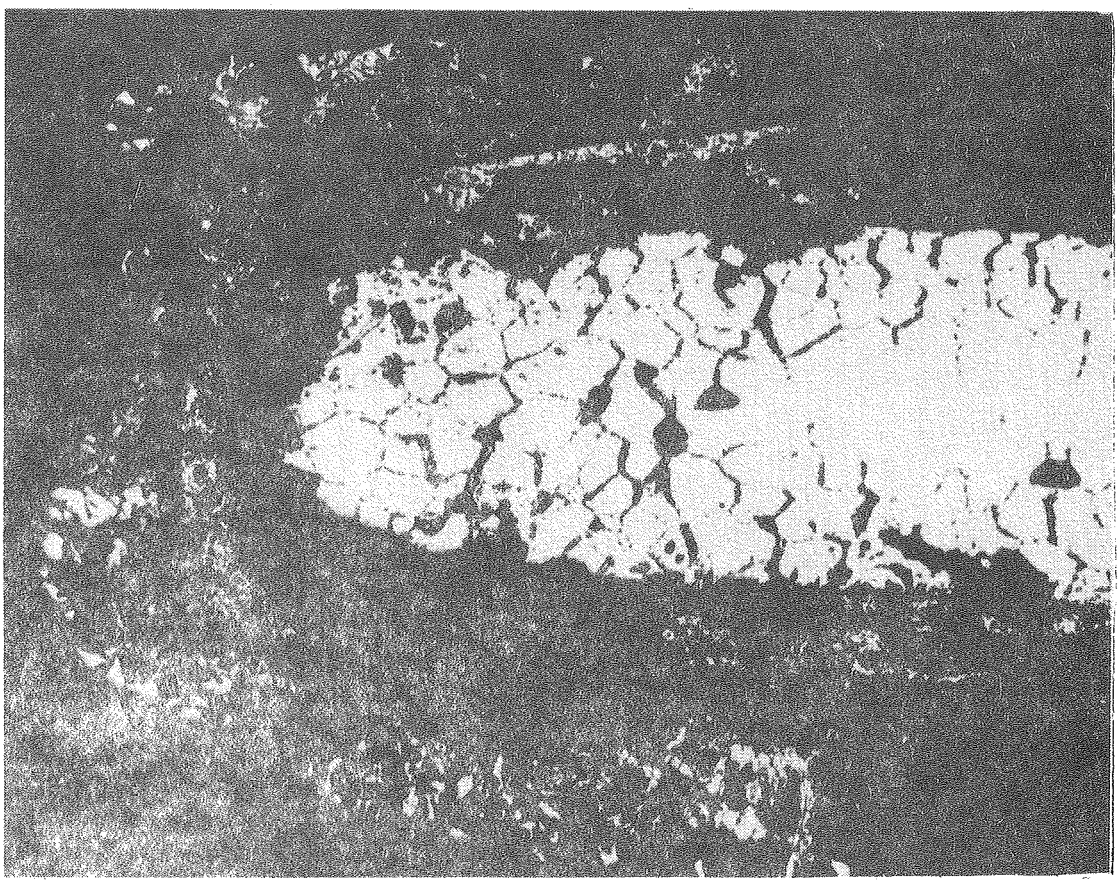

XBB 781-190

Fig. 16. The optical micrograph, magnified 40X, of the cross section of Fe-15Cr-10Al alloy corroded for 2 days. The specimen has been completely corroded.

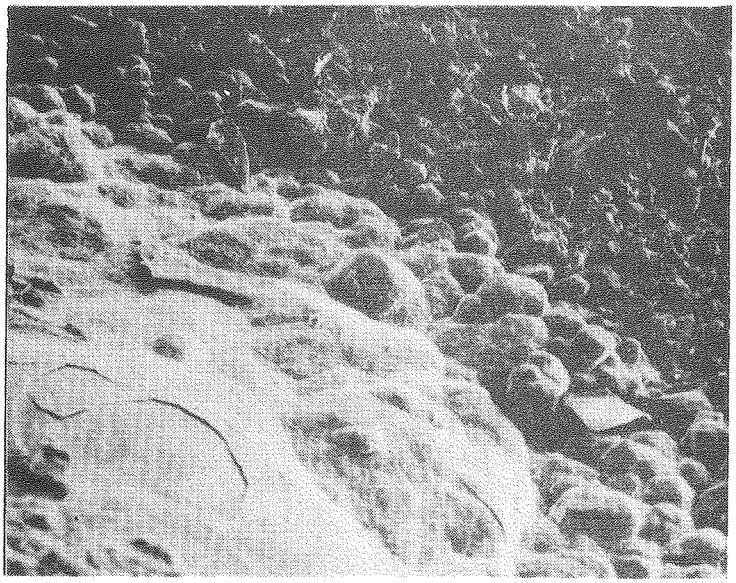

A

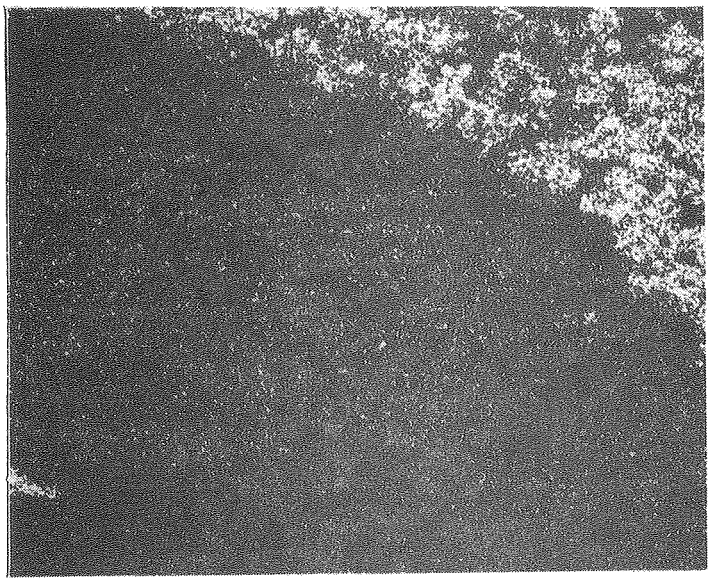

B

XBB 770-12690

Fig. 17. The top surface of a specimen of Fe-18Cr-1.5Si alloy, magnified 200X, corroded for 1 day. "A" is the secondary electron image of the outer surface, and "B" is the x-ray image for S. The micrographs reveal that sulfides are formed on the surface of the specimen within a day of corrosion. Areas which are not rich in S are particles of Cr_2O_3.

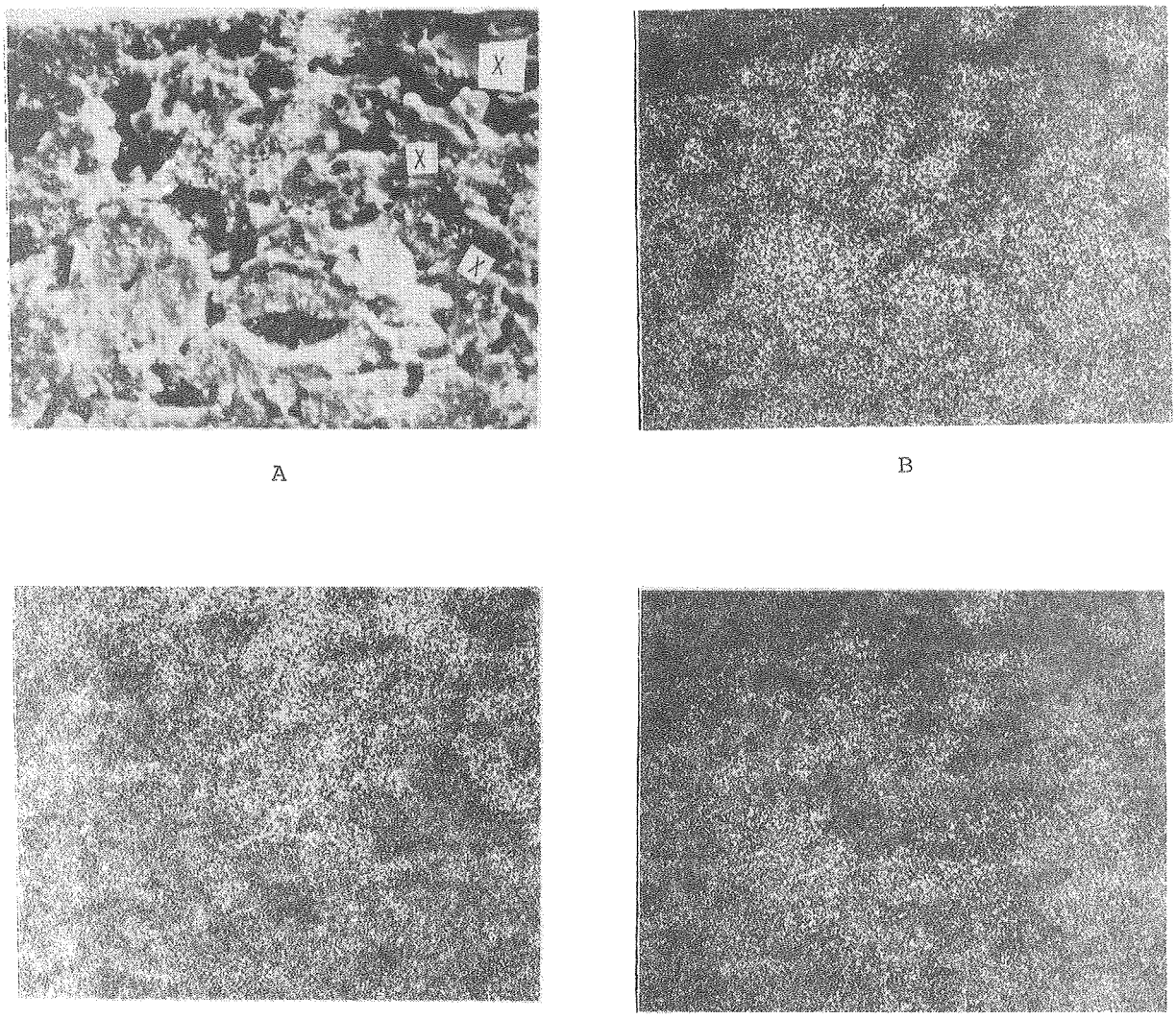

XBB 784-4725

Fig. 18. An area near the scale/alloy interface of an alloy containing 1-5 Si corroded for 2 days. "A" is the secondary electron image magnified at 2KX, and "B", "C", and "D" show the iron, sulfur, and chromium maps respectively. The Cr_2O_3 scale near the metal interface is interspersed with sulfide channels, as indicated by the "X"'s in the electron image.

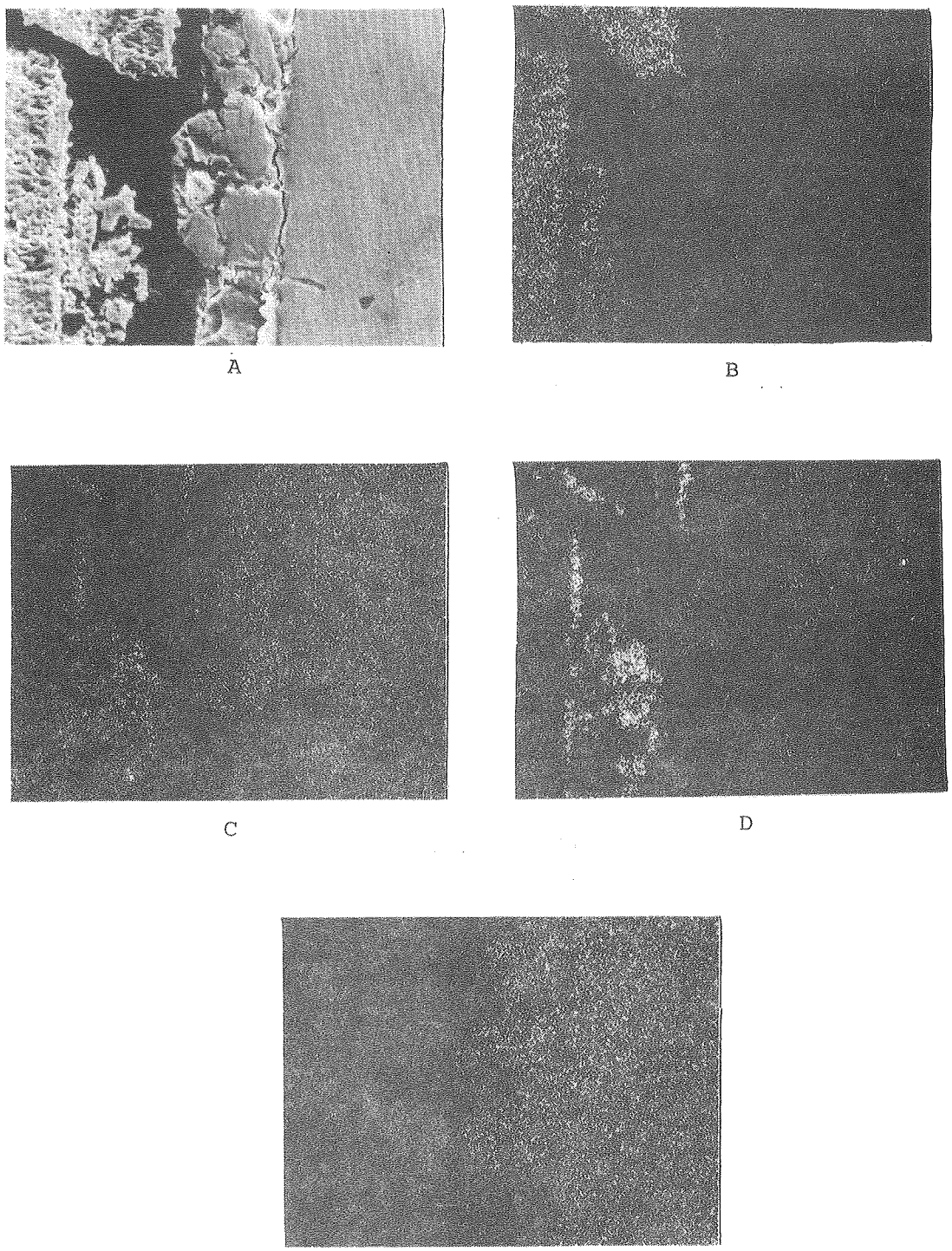

XBB 770-12691

Fig. 19. The scale/alloy interface of a specimen of Fe-15Cr-10Al alloy, magnified 130X, corroded for 3 days. "A" is the secondary electron image of the scale/alloy interface, "B" is the x-ray map for Al, "C" is the x-ray map for Cr, "D" is the x-ray map for S, and "E" is the x-ray map for Fe. Note the formation of Cr-rich sulfides within and beneath the Al_2O_3 scale, which is very porous.

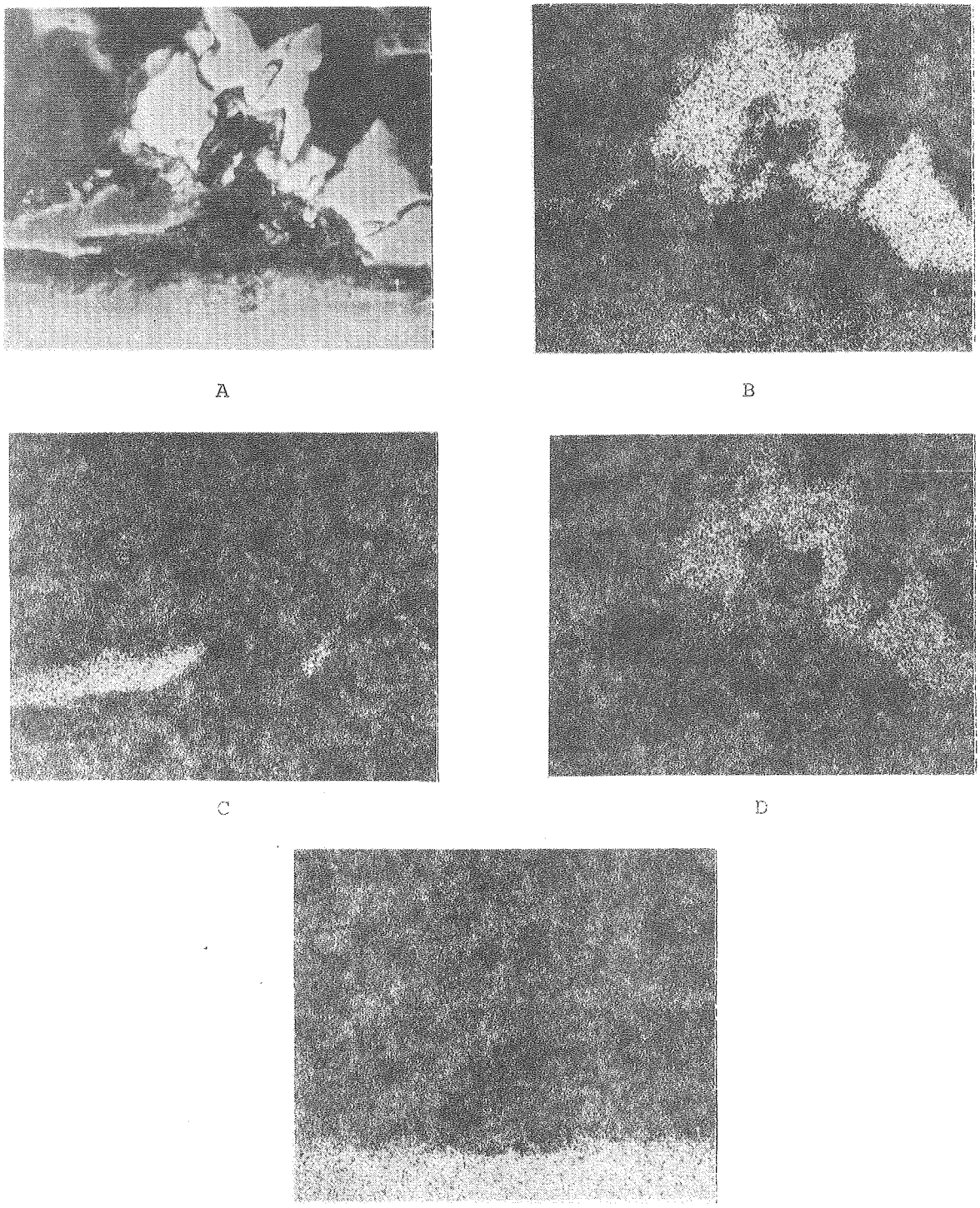

Fig. 20. Evidence for the formation of duplex Cr_2O_3/Al_2O_3 scale. "A" is the secondary electron image of a specimen of Fe-18Cr-5Al corroded for 5 days. Magnification is 2KX. "B", "C", "D", and "E" show Cr, Al, S, and Fe x-ray maps respectively. The x-ray maps for Cr and S show a region rich in Cr, but containing no S. This region is Cr_2O_3 and is present on top of the Al_2O_3 scale. Sulfur has not penetrated the Cr_2O_3/Al_2O_3 duplex scale, but has penetrated the single Al_2O_3 scale.

This report was done with support from the Department of Energy. Any conclusions or opinions expressed in this report represent solely those of the author(s) and not necessarily those of The Regents of the University of California, the Lawrence Berkeley Laboratory or the Department of Energy.